

YAP promotes cell-autonomous immune responses to tackle intracellular *Staphylococcus aureus* in vitro

Received: 11 March 2022

Accepted: 24 October 2022

Published online: 16 November 2022

 Check for updates

Robin Caire ^{1,2} ✉, Estelle Audoux ^{1,2}, Mireille Thomas³, Elisa Dalix³, Aurélien Peyron ^{1,2}, Killian Rodriguez ^{1,2}, Nicola Pordone ^{1,2}, Johann Guillemot ^{1,2}, Yann Dickerscheit ^{1,2}, Hubert Marotte ³, François Vandenesch ^{4,5}, Frédéric Laurent^{4,5}, Jérôme Josse ⁴ & Paul O. Verhoeven ^{1,2,6} ✉

Transcriptional cofactors YAP/TAZ have recently been found to support autophagy and inflammation, which are part of cell-autonomous immunity and are critical in antibacterial defense. Here, we studied the role of YAP against *Staphylococcus aureus* using CRISPR/Cas9-mutated HEK293 cells and a primary cell-based organoid model. We found that *S. aureus* infection increases YAP transcriptional activity, which is required to reduce intracellular *S. aureus* replication. A 770-gene targeted transcriptomic analysis revealed that YAP upregulates genes involved in autophagy/lysosome and inflammation pathways in both infected and uninfected conditions. The YAP-TEAD transcriptional activity promotes autophagic flux and lysosomal acidification, which are then important for defense against intracellular *S. aureus*. Furthermore, the staphylococcal toxin C3 exoenzyme EDIN-B was found effective in preventing YAP-mediated cell-autonomous immune response. This study provides key insights on the anti-*S. aureus* activity of YAP, which could be conserved for defense against other intracellular bacteria.

Yes-associated protein (YAP) and transcriptional co-activator with PDZ-binding motif (TAZ) are transcriptional co-factors involved in many basic cellular functions. YAP and TAZ could interact with TEA domain (TEAD) transcription factor, their main transcriptional partner, to elicit target gene expression^{1,2}. This interaction occurs through the TEAD-binding domain (TBD) of YAP, which is highly conserved throughout evolution^{3,4}. The Hippo pathway was the first described mechanism for YAP/TAZ phosphorylation that leads to its cytoplasmic retention or proteasomal degradation^{5,6}. Additionally, YAP/TAZ act as major mechanotransducers that integrate mechanical *stimuli* into

transcriptional responses⁷. The subcellular localization and nuclear translocation of YAP are regulated by the Rho family of GTPases and actin tension^{7–9}. At low cell density, YAP exists in the nucleus and is transcriptionally active, whereas at high cell density, it remains in the cytoplasm⁸. The YAP/TAZ transcriptional program has been extensively studied in cancer research because it promotes cancer cell survival, proliferation, and invasiveness¹⁰. Growing evidence suggests that YAP/TAZ are inflammation-responsive and promote inflammation, as well as immune pro-inflammatory cell differentiation^{11–13}. Recent studies have highlighted the role of YAP/TAZ in autophagy through the

¹CIRI, Centre International de Recherche en Infectiologie, GIMAP team, Université de Lyon, Inserm, U1111, CNRS, UMR5308, ENS Lyon, Université Claude Bernard Lyon 1, Lyon, France. ²Faculty of Medicine, Université Jean Monnet St-Etienne, St-Etienne, France. ³SAINBIOSE, U1059-INSERM, Université Jean Monnet St-Etienne, St-Etienne, France. ⁴CIRI, Centre International de Recherche en Infectiologie, StaPath team, Université de Lyon, Inserm, U1111, CNRS, UMR5308, ENS Lyon, Université Claude Bernard Lyon 1, Lyon, France. ⁵Department of Bacteriology, Institute for infectious Agents, Hospices Civiles de Lyon, Lyon, France. ⁶Department of Infectious Agents and Hygiene, University Hospital of St-Etienne, St-Etienne, France. ✉ e-mail: caire.robin@gmail.com; paul.verhoeven@univ-st-etienne.fr

transcription of genes encoding proteins involved in the formation of autophagosomes or their fusion with lysosomes^{14,15}. Autophagy against intracellular pathogens (also known as xenophagy) is used by virtually all cell types. Autophagy and inflammation are conserved cell-autonomous responses that restrict infection and increase specialized immune cell recruitment for pathogen clearance^{16,17}. Despite its involvement in autophagy and inflammation, the modulation and role of YAP during bacterial infections remain poorly investigated, and the findings are somewhat controversial. *Helicobacter pylori* infection in gastric cells (in vitro) leads to YAP transcriptional activation and inflammation (increased IL-1 β expression), which, in turn, promotes tumorigenesis¹⁸. YAP transcriptional activity in B cells has been found to promote inflammasome activation and likely contribute to defense against *Salmonella* infection in vitro¹⁹. In a mouse model *Streptococcus pneumoniae*-based pneumonia, alveolar cells exhibited increased YAP/TAZ activity, which is important for tissue healing as well as reducing NF- κ B activity²⁰. In *Caenorhabditis elegans* and mice, YAP is required to control intestinal infection by *Pseudomonas aeruginosa* and *Salmonella enterica* serovar Typhimurium²¹. In contrast, Yorkie (YAP homolog in *Drosophila melanogaster*) transcriptional activity was found to inhibit the production of antimicrobial peptides by inhibiting NF- κ B activity and fostering infection with gram-positive bacteria²². In addition, indirect observations could link YAP and bacterial infections. Indeed, C3 exoenzyme ADP-ribosyltransferase, a bacterial toxin secreted by *Clostridium botulinum*, is known to be a highly specific RhoA inhibitor²³. This commercially available toxin is commonly used to inhibit YAP activity in vitro⁷. It is also noteworthy that many intracellular bacterial species can produce C3-like and other toxins that are potent RhoA inhibitors^{24,25}. For instance, epidermal cell differentiation inhibitors (EDINs) produced by *Staphylococcus aureus* belong to the *C. botulinum* C3 exoenzyme family of bacterial ADP-ribosyltransferases²⁶. The EDIN-B-expressing *S. aureus* clone ST80-MRSA-IV was found to inhibit RhoA activity in vitro²⁷. In humans, the prevalence of *edin*-positive *S. aureus* strains is associated with deep-seated soft tissue infections, suggesting that EDINs increase the virulence of *S. aureus* in vivo²⁸. Despite the strong ability of the C3 exoenzyme to inhibit YAP transcriptional activity, whether the intracellular production of C3 exoenzymes, such as EDINs, can foster *S. aureus* infection through YAP inhibition remains unknown.

Staphylococcus aureus is both a commensal and life-threatening human pathogen responsible for various infections, such as soft skin tissue infections, bacteremia, endocarditis, and osteoarticular infections²⁹. It is widely recognized as a facultative intracellular bacterium capable of triggering its internalization inside non-professional phagocytic cells (NPPCs) by interacting with different host cell receptors³⁰. Inside the host cell, *S. aureus* has been found to be engulfed in autophagosomes by selective autophagy involving cargo receptor proteins, such as sequestosome 1 (SQSTM1/P62), restricting intracellular *S. aureus*³¹. Autophagy has been shown to be a critical mechanism in defense against *S. aureus* infection in mice and zebrafish^{32,33}.

In this study, we investigated the potential antibacterial role of the YAP-TEAD transcriptional program using *S. aureus* infection in HEK293 cells and synovial organoid-based models. We demonstrate that YAP-TEAD transcriptional activity is involved in xenophagy as it enhances autophagic flux to promote *S. aureus* clearance. Further, we show that YAP mediates the expression of host response genes that are known to be important for clearing bacterial infections. In addition, we demonstrate that EDIN-B-producing *S. aureus* prevents YAP-TEAD transcriptional activity to foster its intracellular replication.

Results

Staphylococcus aureus infection elicits YAP transcriptional activity prevented by the expression of the *edinB* gene

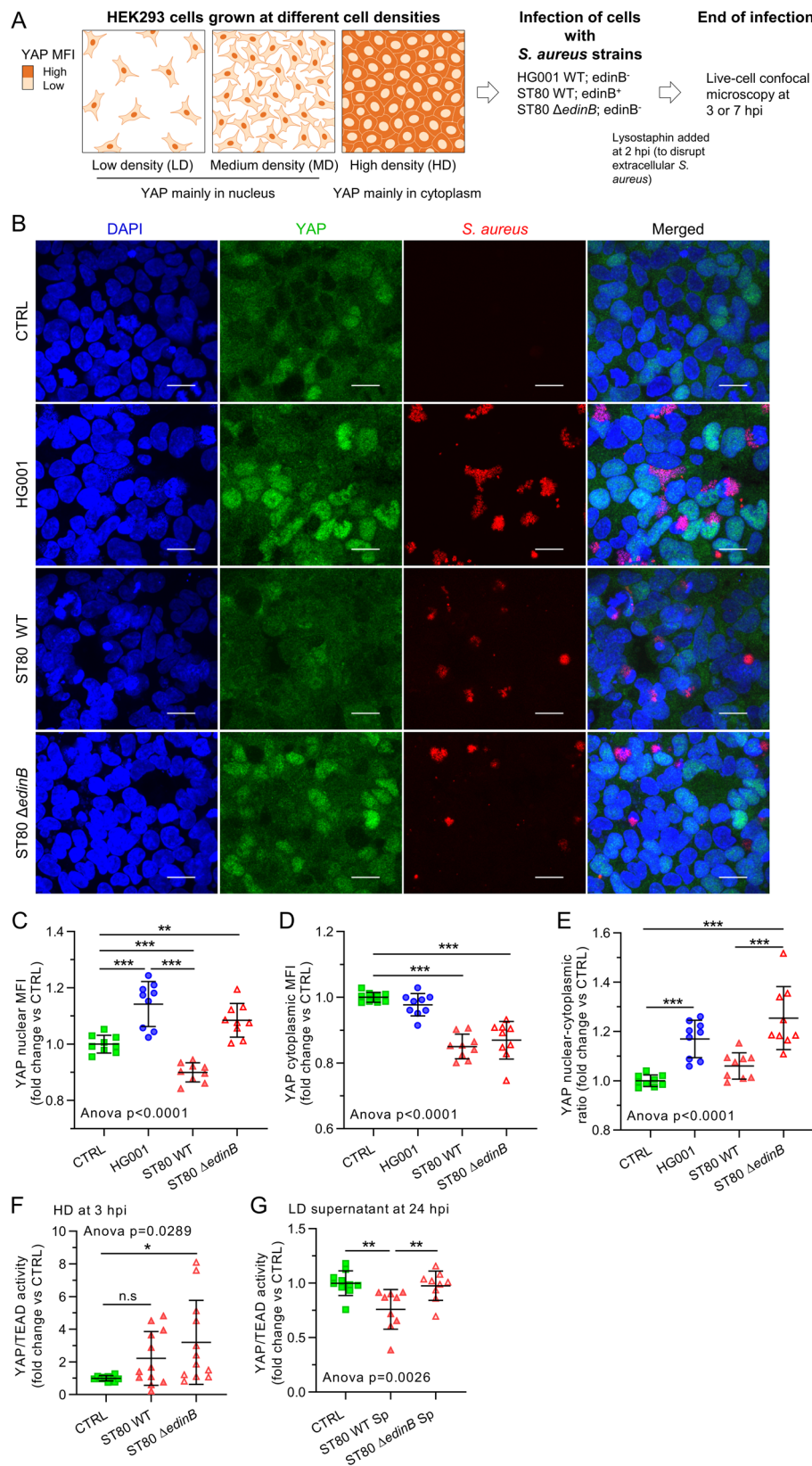
In this study, we used a lysostaphin (a non-cell permeable bacteriocin active against *S. aureus*) protection assay-based model³⁴ to focus on

intracellular bacteria and avoid uncontrolled extracellular bacterial replication.

To investigate YAP signaling in response to *S. aureus* infection, we first used the HG001 *S. aureus* strain (that lacks *edin* genes) in HEK293 cells at different cell densities. The workflow of the experimental procedure is illustrated in Fig. 1A. At high cell density (HD), YAP was mainly cytoplasmic, as expected (Fig. 1B). In this scenario, *S. aureus* induced an increase in YAP nuclear mean fluorescence intensity (MFI) but not in cytoplasmic MFI, resulting in an increase in the YAP nuclear/cytoplasmic (NC) ratio at 7 h post-infection (hpi) (Fig. 1B–E). In contrast, at low cell density (LD) (i.e., when cells are completely isolated from each other, and YAP is exclusively localized in the nucleus) YAP remained localized in the nucleus upon *S. aureus* infection (Supplementary Fig. 1A). Immunoblotting showed that *S. aureus* did not change YAP and TAZ total protein levels at medium cell density (MD) (i.e., when cells formed few contacts and YAP was mainly localized in the nucleus) (Supplementary Fig. 1B–D). In MD, neither the activity of TEAD nor the expression of cysteine-rich inducer 61 (*CYR61*), which is a YAP/TAZ-TEAD target gene, was modified upon *S. aureus* infection (Supplementary Fig. 1E–G). Thus, *S. aureus* HG001 strain infection was found to trigger YAP nuclear translocation but did not enhance YAP signaling when it was already active. We then tested whether the C3 exoenzyme EDIN-B secreted by the *S. aureus* ST80-MRSA-IV strain could prevent YAP activation. Given that the *edinB*-encoded C3 exoenzyme is a membrane non-permeable toxin³⁵, cells were incubated with *S. aureus* culture supernatants for 24 h to allow the toxin to enter cells. We found that the culture supernatant of the ST80 wild-type (WT) strain reduced the nuclear and cytoplasmic localization of YAP, resulting in a decrease in the YAP NC ratio in cells at HD (Supplementary Fig. 2A–D) and an inhibition of TEAD transcriptional activity at LD (Fig. 1G). In contrast, the culture supernatant of the *edinB*-deleted ST80-MRSA-IV strain (ST80 Δ *edinB*) had no effect on YAP localization and TEAD activity (Fig. 1G and Supplementary Fig. 2A–D). Together, these results demonstrate that *S. aureus* EDIN-B toxin is highly effective in inhibiting YAP-TEAD activity. *Staphylococcus aureus* has been shown to be more efficient in delivering EDIN-B directly into the host cell after internalization³⁵. Consequently, we tested whether infection with the ST80 WT and ST80 Δ *edinB* strains modulates YAP subcellular localization and transcriptional activity. As expected, the ST80 Δ *edinB* strain was found to enhance YAP nuclear intensity and decrease YAP cytoplasmic intensity, resulting in a strong increase in the YAP NC ratio (Fig. 1B–E) at 7 hpi in HD cells. In contrast, the EDIN-B-expressing ST80 WT strain was found to reduce YAP nuclear MFI and NC ratio compared to ST80 Δ *edinB* at 7 hpi in HD cells as well as YAP cytoplasmic and nuclear MFI compared to the control cells (Fig. 1B–E). In addition, ST80 Δ *edinB* was found to increase TEAD transcriptional activity as soon as 3 hpi in HD cells, whereas it was not the case with the ST80 WT strain (Fig. 1F). These results demonstrated that the *S. aureus* infection (but not the *S. aureus* supernatant) caused an increase in YAP nuclear localization and YAP-TEAD transcriptional activity in vitro. Interestingly, the EDIN-B-expressing ST80 WT strain as well as the EDIN-B toxin alone were found to be effective in preventing or decreasing YAP activity.

YAP transcriptional activity is required to limit the intracellular replication of *S. aureus*

As YAP is activated during infection, we investigated whether YAP-TEAD transcriptional activity was needed to fight *S. aureus* in vitro. We used WT and YAP-deleted (YAP^{-/-}) HEK293 cells generated using the CRISPR-Cas9 technique³⁶. YAP knockout was confirmed by immunoblotting, and the absence of YAP transcriptional activity was confirmed by a decrease in *CYR61* expression by RT-qPCR (Supplementary Fig. 1B, C, G). Of note, YAP knockout slightly decreased TAZ total protein levels (Supplementary Fig. 1B, D), thus, ruling out the notion that TAZ overexpression compensates for YAP deletion in our model. To



specifically investigate the role of YAP-TEAD activity, we engineered HEK293 cells with a heterozygote mutation of YAP within its TEAD-binding domain (YAP Δ TEAD^{-/+}) that resulted in the substitution of four amino acids (Fig. 2A) critical for binding to TEAD⁴. In LD cells, YAP-TEAD activity was strongly decreased in YAP Δ TEAD^{-/+} cells compared to WT cells (Fig. 2B). Subsequent experiments were performed at MD

to have a robust basal activity of YAP in WT cells, compared to YAP-mutated cells (i.e., YAP^{-/-} and YAP Δ TEAD^{-/+} cells). Using the DsRed-expressing *S. aureus* HG001 strain, we first observed by confocal microscopy that the volume corresponding to the DsRed fluorescence (i.e., *S. aureus* volume) was increased between 3 and 7 hpi, indicating that *S. aureus* was replicating inside the cell. Strikingly, the increase in

Fig. 1 | *Staphylococcus aureus* toxin EDIN-B prevented YAP activation in HEK293 cells. **A** Experimental design used during infection in HEK293 cells. HEK293 cells were cultured at high (**B–F**) or low density (**G**). HG001 or ST80 *S. aureus* infection was at a multiplicity of infection of 10 for 7 h (**B–E**) or 3 h (**F**). *S. aureus* were allowed to contact for 2 h with the cells, and lysostaphin was added at 10 µg/mL for the rest of the experiments to avoid extracellular *S. aureus* multiplication. **B** Confocal representative z-stack max intensity projection images of YAP (immunolabeling, green), nuclei (Hoechst, blue), and DsRed-expressing *S. aureus* (red). Scale bar: 20 µm. **C–E** Quantification of YAP nuclear mean fluorescence intensity (MFI) (**C**), YAP cytoplasmic MFI (**D**), and YAP nuclear cytoplasmic ratio (**E**)

of HG001-infected cells ($n = 9/\text{group}$). **F, G** Luciferase reporter assay of TEAD transcription factor activity ($8 \times \text{GTIC}$) for ST80 *S. aureus* infection (**F**) or ST80 strain supernatant treatment for 24 h (**G**) (**F** CTRL $n = 10$, ST80 WT $n = 12$, ST80 ΔedinB $n = 12$; **G** $n = 9/\text{group}$). Results were expressed as fold change vs. control group and presented as individual values with mean \pm SD, representing three independent experiments. CTRL control, WT wild-type, ST80 ΔedinB EDIN-B-deleted ST80 strain, Sp supernatant. One-way Analysis of variance (ANOVA) test with false discovery rate (FDR) correction for multiple comparisons post hoc tests: * $p < 0.05$; ** $p < 0.01$; *** $p < 0.001$.

S. aureus intracellular volume was more pronounced in both YAP^{-/-} and YAP $\Delta\text{TEAD}^{+/+}$ cells, with the presence of heavily infected cells (Fig. 2C, D). These results were confirmed by quantifying intracellular *S. aureus* loads on agar plates (Fig. 2E). Interestingly, in WT cells, the increase in intracellular volume of the ST80 WT strain was more pronounced than that of the ST80 ΔedinB strain, showing that EDIN-B expression was an advantage for *S. aureus* intracellular replication in vitro (Fig. 2C, F). To further confirm that RhoA-inhibiting toxins conferred bacterial advantage through YAP inhibition, we performed two complementary experiments. First, we showed that addition of the C3 cell permeable toxin (originating from *C. botulinum*) during HG001 infection markedly enhanced *S. aureus* HG001 intracellular volume between 3 and 7 hpi in WT cells, while no further effect was observed in YAP^{-/-} cells (Supplementary Fig. 3A, B). Second, we showed that ST80 ΔedinB readily replicated in YAP^{-/-} cells as efficiently as the ST80 WT strain (Supplementary Fig. 3A, C), suggesting that EDIN-B toxin does not provide any additional benefit to *S. aureus* in the absence of YAP. Taken together, these results indicate that YAP-TEAD activity is required to prevent *S. aureus* intracellular replication and that toxins targeting the Rho family of GTPases (e.g., EDIN-B from *S. aureus*) effectively increase *S. aureus* intracellular growth through YAP inhibition.

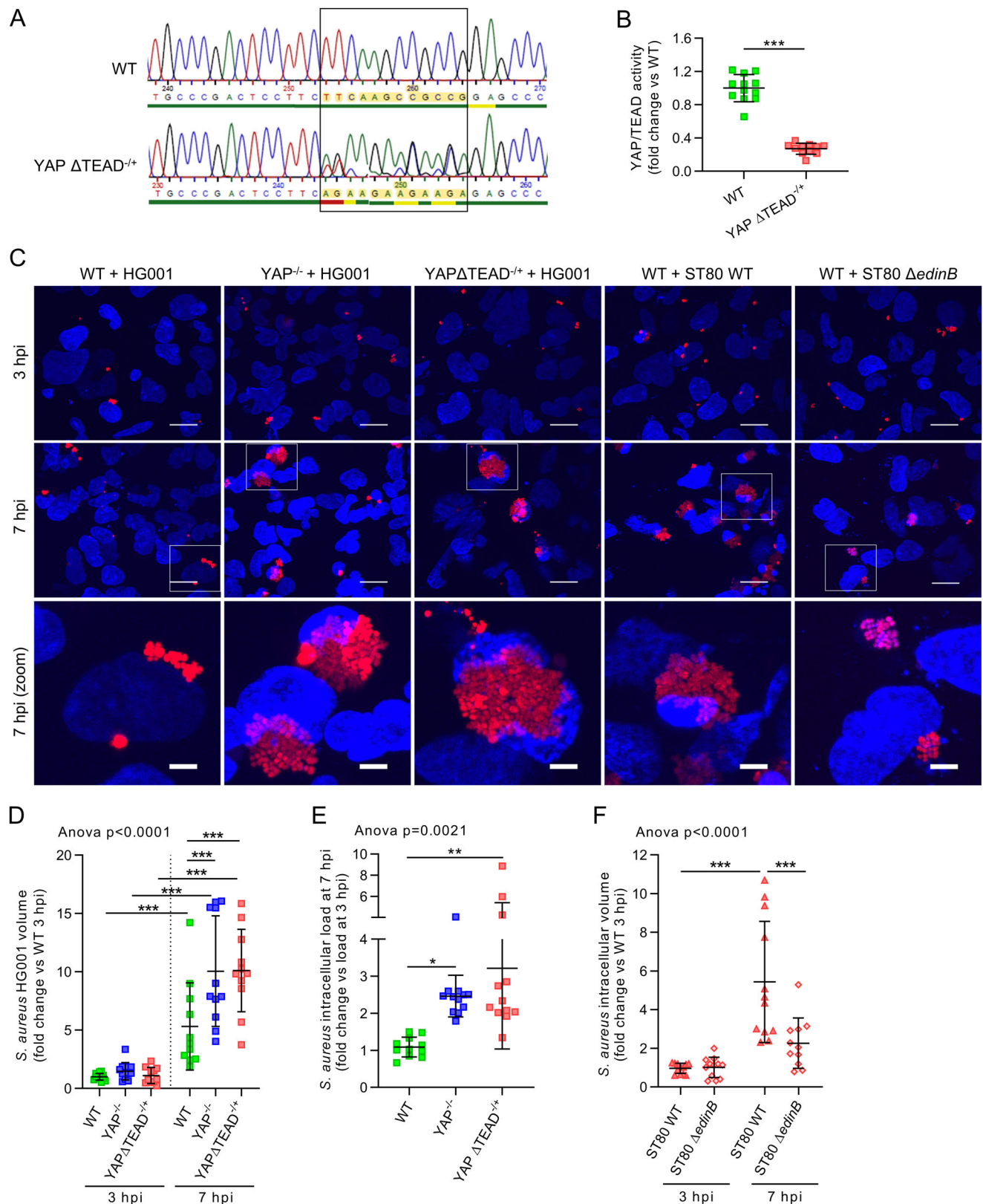
YAP is critical to promote the expression of host response genes usually induced by *S. aureus* infection

To understand why YAP transcriptional activity was important in inhibiting *S. aureus* intracellular replication, we analyzed the expression of 770 genes involved in host response in control or HG001-infected WT or YAP^{-/-} cells at 7 hpi and at MD using the nCounter host response panel. Since we showed that *S. aureus* did not increase YAP activity at this cell density, we focused more on the differences between YAP^{-/-} and WT cells in both uninfected and infected conditions.

Striking differences were observed between WT and YAP^{-/-} cells under both uninfected and infected conditions. For instance, 240 genes were downregulated, whereas only 52 were upregulated in YAP^{-/-} infected cells compared to WT infected cells. Most of the downregulated signaling pathways in YAP^{-/-} cells were inflammation-related signaling pathways (e.g., chemokine, interleukin, inflammasome, and prostaglandin signaling pathways) (Fig. 3A). Upon *S. aureus* infection in WT cells, a pro-inflammatory response profile was induced, whereas in YAP^{-/-} cells, this response was induced but remained at lower levels than that in WT control or infected cells (Fig. 3A). At the level of individual genes, those encoding pro-inflammatory cytokines and chemokines, such as IL-11, CXCL8, and LIF, were among the most downregulated genes in YAP^{-/-} infected cells compared to WT infected cells (Fig. 3B). In a few upregulated genes in YAP^{-/-} infected cells compared to WT infected cells, we detected lysosomal genes such as *LAMP1*, *NPC2*, and *GBA* (Fig. 3B). In YAP^{-/-} cells, we found an upregulation of the lysosome pathway and a downregulation of the autophagic pathway (Fig. 3A), which are known to reduce the intracellular replication of *S. aureus*. Altogether, these results indicate the involvement of YAP in host response gene expression and its contribution to transcriptional immune response in HEK293 cells, consistent with the gene expression profile induced by *S. aureus* infection.

YAP-TEAD transcriptional activity regulate autophagic flux and lysosomal acidification

We then decided to focus on the modulation of autophagy and lysosome signaling pathways by YAP activity in non-infected conditions since these processes are critical for defense against intracellular bacteria. In our model, the overall increase in the lysosome signaling pathway in YAP^{-/-} cells was mainly due to an increased expression of genes encoding lysosomal membrane proteins, which could be used as lysosome markers (e.g., *LAMP1*, *NPC2*, and *GBA*) (Fig. 4A). In contrast, we found decreased expression of several genes related to lysosomal functions. Indeed, we found a decrease in the expression of the *APIS2* and *APIG1* genes encoding adaptins that are involved in lysosomal enzyme transport from the trans-Golgi network to lysosomes³⁷. Furthermore, we observed a downregulation in the expression of cathepsin L (*CTSL*) and *W* and an upregulation in the expression of cathepsin A and Z. A previous study has shown that *CTSL* inhibition leads to LC3-II accumulation and lysosomal enlargement in macrophages³⁸. In addition, we found that *ATP6VOD1*, a gene encoding a subunit of the V-ATPase lysosomal pump critical for lysosomal acidification and autophagy³⁹, was downregulated in YAP^{-/-} cells (Fig. 4A and Supplementary Fig. 4A). Interestingly, a chromatin immunoprecipitation assay using next-generation sequencing (ChIP-seq) data from previous reports⁴⁰ revealed YAP/TAZ-TEAD peaks at active enhancer sites of the *ATP6VOD1*, *ATP6VOA1*, *ATP6VIC1*, and *ATP6VOB* genes⁴⁰. Thus, this transcriptional profile indicates potential lysosome defects in YAP^{-/-} cells that are modulated by YAP-TEAD transcriptional activity. In addition, several autophagy-related genes, including *MAP1LC3A* (encoding microtubule-associated protein 1 light chain 3 alpha (LC3A) protein), *ATG12* (involved in autophagosome elongation through the LC3-I to LC3-II lipidation), and *ATG13* (involved in autophagosome formation), were downregulated. In addition, we observed an upregulation in *ATG10* (involved in the formation of the ATG5-ATG12-ATG16L elongation complex) that probably compensates for *ATG12* downregulation (Fig. 4A and Supplementary Fig. 4A). This profile argued for default autophagosome formation and elongation in YAP^{-/-} cells. YAP/TAZ are known to control the expression of actin-related tension proteins *MLC2* and *DIAPH1*, which are important for autophagosome formation¹⁴. However, we did not evaluate these genes in this work given that we recently showed that *MLC2* expression was not detected in HEK293 cells and *DIAPH1* expression was similar in HEK293 WT and YAP^{-/-} cells⁴¹. To confirm the findings of the transcriptional analysis, we monitored autophagic flux in WT, YAP^{-/-}, and YAP $\Delta\text{TEAD}^{+/+}$ cells. The immunoblotting assay showed no significant differences in basal conditions between WT and YAP^{-/-} cells for LC3-I and LC3-II protein level (Fig. 4B, C). Cell treatment with chloroquine (CQ) (a lysomotropic agent that induces lysosome alkalization and autophagic flux blockage) alone or in combination with rapamycin (autophagy inducer) induced a strong autophagy flux blockage in WT and YAP^{-/-} cells, as evidenced by an increase in the LC3-II/LC3-I ratio compared to untreated cells (Fig. 4B, C). Treatment with CQ alone or in combination with rapamycin highlighted a deficit in LC3-I protein in YAP^{-/-} cells compared to WT cells (corroborating our transcriptomic results) associated with a discrete lower level of LC3-II (Fig. 4B, C). Interestingly, the LC3-II / LC3-I ratio was not different between WT and



$YAP^{-/-}$ cells in CQ-treated cells and was higher in $YAP^{-/-}$ cells compared to WT cells in CQ and rapamycin treated cells (Fig. 4B, C). Thus, highlighting no LC3 lipidation impairment in $YAP^{-/-}$ cells and possibly a higher flux blockage in those cells. (Fig. 4B, C). To further study autophagy regulation in both models and highlight critical structural changes that cannot be detected with WB, we used live-cell confocal microscopy and a CYTO-ID probe to label autophagic vesicles in living

cells. In basal conditions, we detected few autophagic vesicles, but they were more abundant and especially much larger in $YAP^{-/-}$ and $YAP\Delta TEAD^{-/-}$ cells than in WT cells (Fig. 4D, E). In YAP -mutated cells, these larger autophagic vesicles also appeared misshapen, in contrast to the spherical vesicles observed in WT cells (Fig. 4D). Similar results were obtained from cells immunolabeled with anti-LC3 antibody (Supplementary Fig. 4B), ruling out an artifact due to the CYTO-ID probe.

Fig. 2 | YAP transcriptional activity inhibits intracellular *Staphylococcus aureus* replication. HEK293 cells were cultured at low (B) or medium density (C–F). HG001 or ST80 *S. aureus* infection was at a multiplicity of infection of 1 for 3 or 7 h, as indicated. *Staphylococcus aureus* were allowed to contact cells for 2 h, and lysostaphin was added at 10 µg/mL for the remaining experiments to avoid extracellular *S. aureus* multiplication. **A** Electropherogram of WT and YAPΔTEAD^{-/-} cells showing TTCAAGCCGCCG replacement by AGAAGAAGA. **B** Luciferase reporter assay of TEAD transcription factor activity (8 × GTIIC) for WT and YAPΔTEAD^{-/-} cells (WT *n* = 12, YAPΔTEAD^{-/-} *n* = 11). **C** Representative confocal z-stack max intensity projection images of live cells labeled with DAPI (nuclei, blue) and infected with DsRed-expressing *S. aureus* HG001 or ST80 strains as indicated (red); scale bar 20 µm and 5 µm for zoomed image. **D** Microscopy quantification of intracellular HG001 mean volume per cell (WT 3 hpi *n* = 13, YAP^{-/-} 3 hpi *n* = 13, YAPΔTEAD^{-/-} 3 hpi

n = 12; WT 7 hpi *n* = 12, YAP^{-/-} 3 hpi *n* = 12, YAPΔTEAD^{-/-} 3 hpi *n* = 12). **E** Quantification of HG001 colony-forming unit (CFU) per mL on an agar plate at a ratio of 3 hpi/7 hpi (WT *n* = 11, YAP^{-/-} *n* = 12, YAPΔTEAD^{-/-} *n* = 12). **F** Microscopy quantification of the intracellular ST80 strain mean volume per cell (ST80 WT 3 hpi *n* = 13, ST80 ΔedinB 3 hpi *n* = 13, ST80 WT 7 hpi *n* = 13, ST80 ΔedinB 7 hpi *n* = 12). For microscopy quantification (D, F), the total *S. aureus* volume measured in the field was divided by the number of nuclei in the same field. Results were expressed as fold change vs. control group and presented as individual values with mean ± SD, representing three independent experiments. WT wild-type, ST80ΔedinB EDIN-B-deleted ST80 strain, CFU colony-forming unit. Unpaired t-test (B) or one-way analysis of variance (ANOVA) test with false discover rate (FDR) correction for multiple comparison post hoc tests: **p* < 0.05; ***p* < 0.01; ****p* < 0.001.

We then performed live-cell microscopy with the SiR-Lysosome probe that specifically labels cathepsin D and consequently lysosomes. The large autophagic vesicles observed in YAP^{-/-} cells were confirmed to be autophagolysosomes (Fig. 4F). Moreover, SiR-Lysosome-labeled vesicles or CYTO-ID and SiR-Lysosome dual-labeled vesicles (i.e., autophagolysosomes) were larger in YAP^{-/-} cells compared to WT cells (Fig. 4F, G). Additionally, the proportion of CYTO-ID and SiR-Lysosome dual-labeled vesicles among all autophagic vesicles was similar in WT and YAP^{-/-} cells, indicating that no fusion issues occurred between autophagosomes and lysosomes (Fig. 4G). These results further confirm the hypothesis that autophagic flux blockage in YAP^{-/-} cells leads to accumulation of larger autophagolysosomes.

Given that lysosomal alkalization induces the accumulation of autophagic vesicles and larger autophagolysosomes³⁹, we treated cells with CQ to induce lysosome alkalization. The resulting large autophagolysosomes in YAP^{-/-} cells were similar to those obtained following WT cell treatment with CQ, even though YAP^{-/-} cells contained significantly fewer vesicles than CQ-treated-WT cells (Fig. 4F). Together with our transcriptomic results, these observations suggest an anomaly in the degradative activity of autophagolysosomes that led us to compare lysosome pH in WT and YAP-mutated cell lines. In basal conditions, no difference was detected between WT, YAP^{-/-}, and YAPΔTEAD^{-/-} cells. Bafilomycin A1, an inhibitor of V-ATPase pumps, was effective in inducing lysosomal alkalization in both cell lines (Fig. 4H, I). However, 20 min after bafilomycin A1 removal, lysosomes reacidification was more efficient in WT cells than in YAP^{-/-} and YAPΔTEAD^{-/-} cells, indicating lysosomal dysfunction in these cells (Fig. 4H, I).

These results showed that YAP-TEAD activity promotes the expression of autophagic and lysosomal genes that are important for normal autophagic flux regulation and lysosomal functions.

Loss of YAP-TEAD transcriptional activity worsens blockage of autophagic flux induced by *S. aureus* and fosters its escape from autophagic vesicles

Internalized *S. aureus* is known to elicit a strong autophagic response in NPPCs, which is required to clear intracellular *S. aureus* by addressing *S. aureus*-containing autophagosomes to lysosomes. Therefore, we decided to investigate how the alteration of autophagy and lysosome signaling pathways observed in YAP-mutated cells could explain the strong replication of intracellular *S. aureus* in these cells.

Transcriptomic analysis of WT and YAP^{-/-} cells infected with *S. aureus* showed that the expression of specific genes involved in autophagy and lysosome signaling pathways were altered in YAP^{-/-} cells (Supplementary Fig. 4A, C). For instance, *CTSL* expression was lower in YAP^{-/-} infected cells compared to WT infected cells (Supplementary Fig. 4A, C, D). To characterize the functional relevance of autophagy and lysosome function for restricting *S. aureus* intracellular replication, we used CQ to increase the lysosome pH and alter the late phase of the autophagic process. In CQ-treated-WT cells, *S. aureus* replication was increased, approaching the *S. aureus* volume measured

in YAP^{-/-} untreated cells, thus confirming the critical role of lysosome pH for controlling infection (Fig. 5A, B). As expected, CQ treatment in YAP^{-/-} cells did not worsen *S. aureus* infection, suggesting that intracellular replication of *S. aureus* in YAP^{-/-} cells was due to autophagy and lysosomal defects (Fig. 5A, B).

In addition, live-cell confocal microscopy was used to assess autophagic responses during *S. aureus* infection. In WT cells, we observed a strong increase in autophagic vesicle count and volume at 3 hpi, whereas at 7 hpi, the volume of autophagic vesicles continued to rise with no further increase in the vesicle count, which is in favor of the blockage of autophagic flux (Supplementary Fig. 5A–C). Interestingly, in WT cells, the colocalization of *S. aureus* with autophagic vesicles was found to decrease between 3 and 7 hpi (Supplementary Fig. 5A, D), which reflects the ability of *S. aureus* to escape from autophagic vesicles (e.g., autophagosomes or autolysosomes) and replicate intracellularly. In some of the WT cells, we also observed disrupted *S. aureus* and diffused red fluorescence within autophagic vesicles, indicating a possible degradative function of autophagolysosomes, which may limit the intracellular replication of *S. aureus* in WT cells (Supplementary Fig. 5A). In contrast, such a pattern of degradation was not observed in YAP^{-/-} and YAPΔTEAD^{-/-} cells, suggesting that lysosomal degradative function is altered in these cells, which is in accordance with our data of transcriptomic and lysosome reacidification assays.

This statement is also supported by the fact that the colocalization of *S. aureus* with autophagic vesicles at 7 hpi in these cells was lower than that observed in WT cells (Supplementary Fig. 5A, D), which reflects *S. aureus* escape from autophagic vesicles. This result did not seem to be due to a defect in autophagy initiation since the autophagic vesicle count increased at 3 hpi compared to non-infected conditions, as it did for WT cells (Supplementary Fig. 5A, B). It is also noteworthy that even if the level of colocalization of *S. aureus* with autophagic vesicles was identical to that of WT cells at 3 hpi in YAP-mutated cells, the autophagic vesicles surrounding *S. aureus* were unusually distorted as compared to the spherical vesicles surrounding each individual *S. aureus* bacterium in WT cells (Supplementary Fig. 5A, D). More importantly, the volume of autophagic vesicles strongly increased at 3 hpi in YAP^{-/-} cells compared to WT infected cells (Supplementary Fig. 5A, C), indicating a further autophagic flux blockage during *S. aureus* infection. In YAPΔTEAD^{-/-} cells, the vesicle volume did not increase further at 3 hpi (Supplementary Fig. 5A, F), which could be explained by the fact that the vesicle volume in uninfected cells was already higher than that in WT and YAP^{-/-} cells. For YAP-mutated cell lines, vesicle count and volume decreased between 3 and 7 hpi, which seems to be due to the disruption of autophagic vesicles by *S. aureus* that did not colocalize with the spherical vesicles but were surrounded by CYTO-ID-labeled residues (Supplementary Fig. 5A–F). Immunoblots showed that the LC3-II/LC3-I ratio was not significantly different during infection in YAP^{-/-} cells compared to WT cells (Supplementary Fig. 6A, B). We then performed similar experiments with WT cells infected with

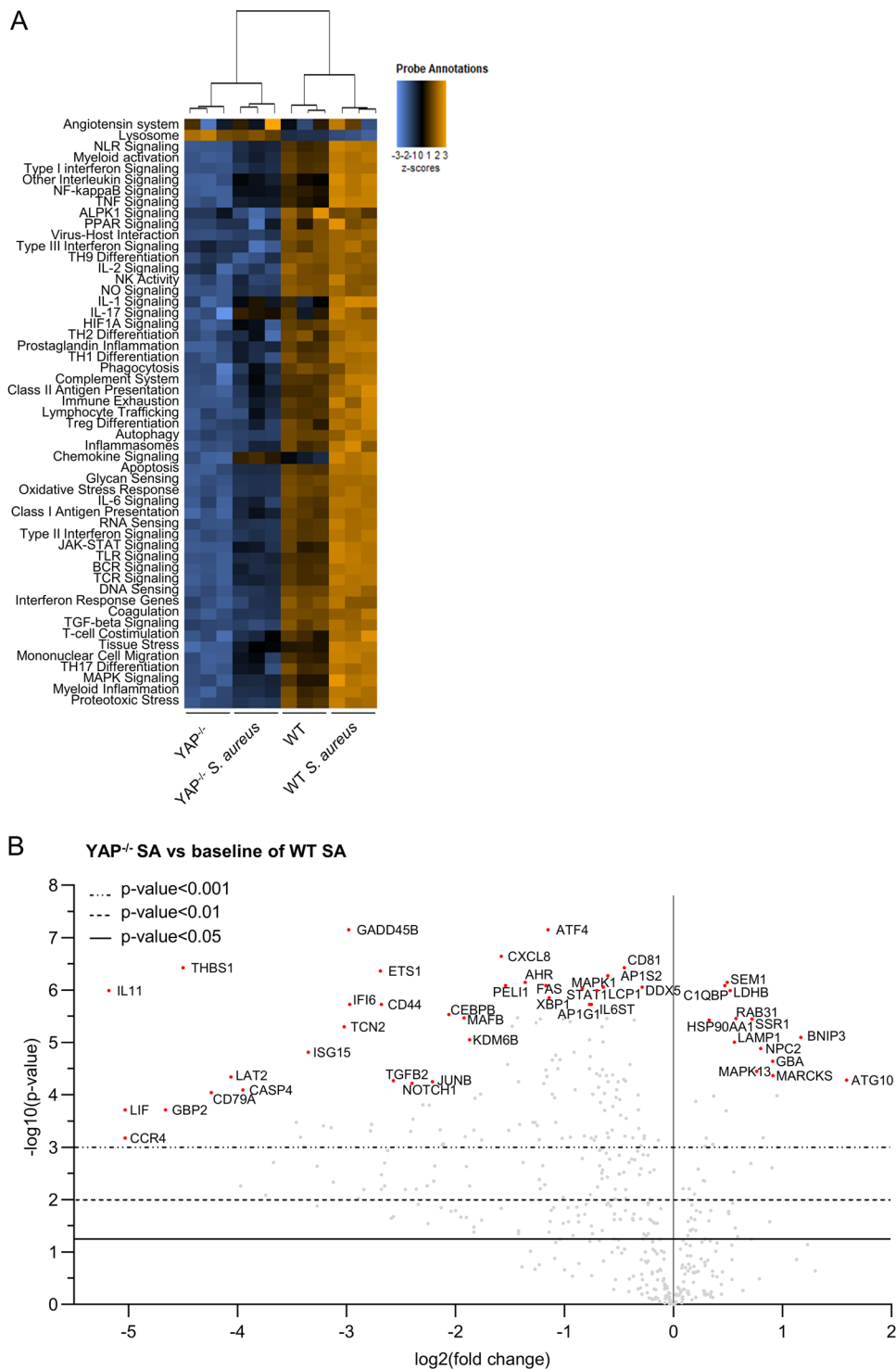
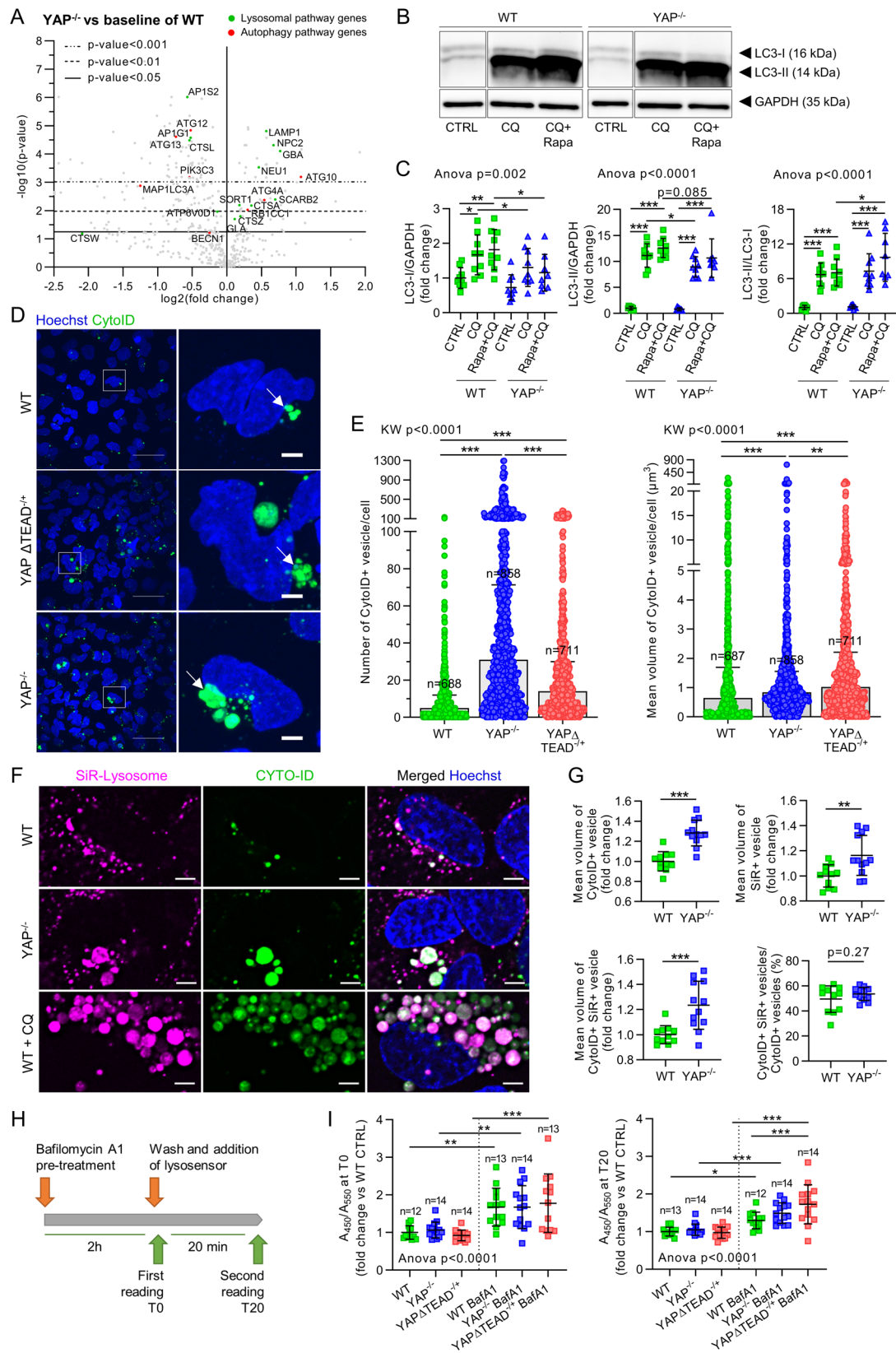


Fig. 3 | YAP promotes host response gene expression important during *Staphylococcus aureus* infection. HEK293 cells were cultured at medium density and infected with HG001 *S. aureus* strain at a multiplicity of infection of 10 for 7 h. *Staphylococcus aureus* were allowed to contact cells for 2 h. Subsequently, lysostaphin was added at 10 μg/mL for the remaining experiments to avoid extracellular *S. aureus* multiplication. **A** Heat map of nCounter NanoString host response pathways; pathways are listed to the left, the most upregulated pathways are depicted in

orange, and the most downregulated pathways are shown in blue; each column corresponds to one sample (n = 3/group). **B** Volcano plot representation of differential gene expression in YAP^{-/-} infected group versus the baseline of WT infected group; depicted genes were the most differentially expressed with the combination of a low p value and a high fold change; p value was calculated with the NanoString software based on t-test corrected with false discovery rate. WT wild-type, SA *S. aureus*.

ST80 WT and ST80 *ΔedinB* strains, both of which were found to enhance vesicle count and volume in a very similar manner (Supplementary Fig. 4A, C). However, the supernatant from the ST80 WT strain induced an increase in autophagolysosome volume compared

to untreated or WT cells treated with ST80 *ΔedinB* supernatant (Supplementary Fig. 7D, E). Although both ST80 WT and ST80 *ΔedinB* strains were found to be highly colocalized in autophagic vesicles at 3 hpi, but the former was able to escape from autophagic



vesicles at 7 hpi in contrast to the latter that remained more confined to autophagic vesicles (Supplementary Fig. 7A, B).

To further elucidate the role of late phase autophagy (i.e., autophagolysosome function), lysosomes were labeled with SiR-Lysosome probe. Autophagic vesicles, as well as SiR-Lysosome-labeled vesicles, were found to be enlarged during infection,

however, to a greater extent in YAP^{-/-} cells compared to WT cells (Fig. 5C–E). Meanwhile, at 7 hpi, the colocalization of *S. aureus* with CYTO-ID-labeled or CYTO-ID and SiR-Lysosome dual-labeled vesicles decreased, indicating that *S. aureus* escaped from both autophagosome and autophagolysosomes (Fig. 5C, F). Of note, the colocalization of *S. aureus* with SiR-Lysosome-labeled vesicles was slightly lower in

Fig. 4 | YAP-TEAD activity is involved in autophagic flux regulation via lysosomal acidification. HEK293 cells were cultured at medium density and remained uninfected. **A** Volcano plot representation of differential gene expression (nCounter NanoString) in YAP^{-/-} control group versus the baseline of WT control group; depicted genes are autophagic (red) or lysosomal (green) pathway genes differentially expressed. **B, C** Representative immunoblot results of LC3A/B -I and -II, and GAPDH (**B**), with their quantification normalized by GAPDH expression (**C**) (WT $n = 9$; YAP^{-/-} $n = 8$). **D** Representative confocal z-stack max intensity projection images of live cells labeled with Hoechst (nuclei, blue) and CYTO-ID (autophagic vesicles, green). Scale bar: 20 μm (left) and 5 μm (right). **E** Corresponding quantification of the autophagic vesicle count or mean vesicle volume per cell, as indicated. Each point represents one cell (n number of cells analyzed/group). **F** Representative confocal (0.5 μm thick z-stack) images of live cells labeled with Hoechst (nuclei, blue), CYTO-ID (autophagic vesicles, green) and SiR-Lysosome (lysosomes, magenta). Scale bar: 5 μm . Cells were treated with 50 μM CQ for 24 h.

G Corresponding quantification; Mean vesicle volume (vesicle volume/vesicle count) for CYTO-ID-positive, SiR-Lysosome-positive and double-positive vesicles; and proportion of double-positives vesicles among the CYTO-ID-positive vesicles (volume of CYTO-ID-positive and SiR-Lysosome-positive vesicles/volume of CYTO-ID-positive vesicles * 100) (WT $n = 11$; YAP^{-/-} $n = 12$). **H** Timeline of LysoSensor experiment. **I** Relative acidity of lysosomes in control or BafA1-treated cells at T0 and T20. An increase of 450/550 nm ratio is representative of lysosome alkalization (n number of samples/group). Results are expressed as fold change vs. control group (where indicated) and presented as individual values with mean \pm SD (**C, I**) or median with interquartile range (**E**), representing three independent experiments. WT wild-type, BafA1 Bafilomycin A1. Unpaired t-test (**G**), one-way analysis of variance (ANOVA) or Kruskal-Wallis (KW) test with false discovery rate (FDR) correction for multiple comparisons post hoc tests: * $p < 0.05$; ** $p < 0.01$; *** $p < 0.001$.

YAP^{-/-} cells, however, this effect was not statistically significant (Fig. 5C, F). Strikingly, *S. aureus* escape from autophagosomes and autolysosomes was nearly complete in YAP^{-/-} cells at 7 hpi (Fig. 5C, F). Collectively, these results confirm that autophagic flux was more impeded in YAP^{-/-} cells than in WT cells during *S. aureus* infection.

Considering that our results suggest that autophagosomal escape is associated with *S. aureus* replication, we exploited the properties of the DsRed fluorescent protein to estimate *S. aureus* replication. Briefly, given that the DsRed maturation time is approximately 26 h⁴², the mean fluorescent intensity (MFI) decreases in rapidly replicating bacteria, while remaining high in slow, or non-replicating, bacteria. At 7 hpi, DsRed-expressing *S. aureus* MFI strongly decreased in YAP^{-/-} cells, indicating a rapid-replicating phenotype inside YAP^{-/-} cells. In contrast, *S. aureus* MFI remained high in WT cells at 7 hpi (Fig. 5C, G). Of note, we observed that bacteria with high fluorescence intensity were localized in autophagolysosome vesicles (Fig. 5C), suggesting that bacterial replication is restricted by these vesicles (or cleared as shown in Supplementary Fig. 5) in WT cells.

Together, these results highlight the critical role of YAP-mediated autophagy to hamper *S. aureus* intracellular growth. More specifically, *S. aureus* takes advantage of autophagy and lysosomal defects observed in YAP-mutated cells, which foster its escape from autophagic (including autophagolysosomes) vesicles, and subsequently initiates intracellular replication. In addition, we showed that EDIN-B-expressing *S. aureus* was more efficient in escaping autophagy, thus suggesting that the YAP-autophagy axis can be targeted by bacterial toxins to foster bacterial intracellular replication.

YAP promotes inflammatory response during *S. aureus* infection

Upon bacterial infection, the cell-autonomous immune response of non-specialized immune cells displays antimicrobial mechanisms^{16,17,43}. An important part of this response is the activation of molecular signaling pathways that enable the expression of inflammatory mediators to attract specialized immune cells for bacterial clearance.

Our transcriptomic analysis highlighted that most of the differences in gene expression between YAP^{-/-} and WT cells were related to inflammatory signaling pathways. Members of the IL-6, IL-11, and LIF signaling pathways were found to be enhanced during *S. aureus* infection in WT cells but remained downregulated in both infected and uninfected YAP^{-/-} cells (Fig. 6A, B). These cytokines support the proliferation and differentiation of hematopoietic stem cells⁴³, and LIF has been shown to enhance the killing of *S. aureus* by neutrophils⁴⁴. Although *IL6* was expressed at low level in the nCounter panel, RT-qPCR showed that *IL6* expression was low in HEK293 cells but was nevertheless increased during *S. aureus* infection in WT cells and remained lower in both infected and uninfected YAP^{-/-} cells (Fig. 6C). The expression of chemokine genes, including *CXCL8*, *CCL20*, *CXCL2*, and *CXCL1*, which are known to enhance immune cell recruitment and are consequently involved in the *S. aureus* inflammatory response,

especially *CXCL8*, which is critical for neutrophil recruitment^{45,46}, was enhanced during *S. aureus* infection in WT cells. Even if these genes were upregulated during *S. aureus* infection in YAP^{-/-} cells, their expression remained strongly downregulated in YAP^{-/-} cells compared to WT cells (Fig. 6A, B). Moreover, the abundance of IL-8 in cell culture supernatants was similar to those obtained for *CXCL8* expression via RT-qPCR, thus, corroborating the nCounter results (Fig. 6C, D). *S. aureus* infection also enhanced the expression of *PTGS2* (also known as cyclooxygenase-2) (Fig. 6A, B), which encodes a key enzyme for the synthesis of prostaglandins that are involved in the inflammatory response against *S. aureus*⁴⁷; however, *PTGS2* expression remained lower in YAP^{-/-} infected and uninfected cells than in WT infected and uninfected cells (Fig. 6A–C). The inflammasome response is important during *S. aureus* infection for neutrophil recruitment⁴⁸. We found that several inflammasome-related genes, such as *CASP4* and *NLRC4*, were downregulated in YAP^{-/-} infected and uninfected cells. In addition, using RT-qPCR the low-level expression of *IL1B* was detected in WT cells during infection, whereas it remained undetectable in YAP^{-/-} infected and uninfected cells (Fig. 6C). Although YAP-TEAD itself could contribute to the expression of cytokines and chemokines, we found that the expression of some transcription factors involved in inflammation was modified in YAP^{-/-} cells. During infection, nuclear factor κB (NF- κB) and activator protein 1 (AP-1) are known to trigger the first inflammatory response in cells⁴⁹. Our results confirmed that *S. aureus* infection triggers NF- κB pathway-related genes but does not increase NF- κB subunits (Supplementary Fig. 6A, B). Likewise, we showed that *S. aureus* infection upregulates MAPK pathway-related genes with increased expression of API members *JUNB* and *FOS* (Supplementary Fig. 6A, B). However, in YAP^{-/-} control or infected cells, we found that these two pathways were highly disrupted due to the downregulation of genes encoding NF- κB subunits (*NFKB1*, *NFKB2*, *REL*, *RELA*, and *RELB*) and API members, including *JUN*, *JUNB*, and *FOS* (Supplementary Fig. 8A, B). Of note, several other inflammatory pathways were altered in YAP^{-/-} cells, with a reduction in interferon signaling, NLR signaling, DNA sensing, and MHC class I signaling (Fig. 3A). Altogether, these results highlight that YAP activity can modulate the expression of a wide range of inflammation-related genes involved in the response against *S. aureus*.

S. aureus ST80 infection in synovial organoids also modulates YAP signaling

Organoid-based infection models enable the study of infection in a 3D cell model using primary cells that display more physiological characteristics than continuous cell lines. In this experiment, we used a model of synovial organoids³⁶, formed with fibroblast-like synovio-cytes (FLSs) from three different donors that were infected with ST80 strains. Given that *S. aureus* is one of the leading causes of osteoarticular infection in humans²⁹, this infection model should be highly clinically relevant.

Fig. 5 | YAP-TEAD transcriptional activity is required to reduce *Staphylococcus aureus*-induced autophagic flux blockage. HEK293 cells were cultured at medium density and infected with *S. aureus* HG001 strain at a multiplicity of infection of 1 for 3 or 7 h, as indicated. *S. aureus* were allowed to contact cells for 2 h, and lysostaphin was added at 10 μ g/mL for the remaining experiments to avoid extracellular *S. aureus* multiplication. **A** Representative confocal 10 z-stack maximum intensity projection images of live cells labeled with Hoechst (nuclei, blue) and infected with DsRed-expressing *S. aureus* HG001 (red); scale bar: 5 μ m. **B** Corresponding quantification of intracellular *S. aureus* HG001 mean volume per cell (WT 3 hpi n = 20, WT + CQ 3 hpi n = 18, YAP^{-/-} 3 hpi n = 21, YAP^{-/-} + CQ 3 hpi n = 17, WT 7 hpi n = 22, WT + CQ 7 hpi n = 16). **C** Representative confocal (0.5 μ m thick z-stack) images of live cells labeled with Hoechst (nuclei, blue), CYTO-ID (Autophagic vesicles, green), and SiR-Lysosome (lysosome, magenta), and infected with DsRed-expressing *S. aureus* HG001 (red); white arrows: *S. aureus* trapped in CYTO-ID and SiR-Lysosome

double-positive vesicles; scale bar: 5 μ m. **D–G** Corresponding microscopy quantifications. Mean vesicle volume (vesicle volume/vesicle count) for CYTO-ID-positive vesicles (**D**) and SiR-Lysosome-positive vesicles (**E**). Relative colocalization between *S. aureus* and CYTO-ID-positive and/or SiR-Lysosome-positive vesicles (**F**); *S. aureus* mean fluorescence intensity (MFI) (**G**) (**D, E**: WT CTRL n = 11, YAP^{-/-} CTRL n = 12, WT 3 hpi n = 16, YAP^{-/-} 3 hpi n = 17, WT 7 hpi n = 18, YAP^{-/-} 7 hpi n = 13; **F**: WT 3 hpi n = 17, YAP^{-/-} 3 hpi n = 18, WT 7 hpi n = 18, YAP^{-/-} 7 hpi n = 13, WT 3 hpi n = 17; **G**: WT 3 hpi n = 13, YAP^{-/-} 3 hpi n = 15, WT 7 hpi n = 16, YAP^{-/-} 7 hpi n = 13). Results are expressed as fold change vs. control group (**B, F, G**) and presented as individual values (each point represents one microscopy field) with mean \pm SD, representing three independent experiments. WT wild-type, CQ chloroquine. Unpaired t-test (**C**), one-way analysis of variance (ANOVA) or Kruskal-Wallis (KW) test with false discovery rate (FDR) correction for multiple comparisons post hoc tests: * p < 0.05; ** p < 0.01; *** p < 0.001.

recognized as a hallmark of synovial inflammation, was found to be mediated through YAP activity^{36,50,51}. At 7 hpi, ST80 Δ edinB induced synovial lining layer thickening (Fig. 7B–D) which suggest that YAP is activated. In contrast, ST80 WT that expressed EDIN-B did not induce an increase in of the synovial lining layer thickness (Fig. 7B–D), probably reflecting YAP inhibition. This assumption was strengthened by the confocal microscopy images showing that the EDIN-B-expressing ST80 WT strain, unlike the ST80 Δ edinB strain, was able to reduce YAP immunolabeling in infected synovial lining layer cells at 7 hpi (Fig. 7E). In addition, the ST80 WT strain was found to inhibit YAP transcriptional activity highlighted by the reduced expression of the connective tissue growth factor (*CTGF*) and *CYR61* genes, whereas the ST80 Δ edinB strain increased their expression (Fig. 7F), which confirmed that the EDIN-B-expressing ST80 WT strain was able to inhibit YAP transcriptional activity in synovial organoids. In addition, since the *CXCL8* and *PTGS2* genes were downregulated in HEK293 YAP^{-/-} infected cells compared to WT infected cells, we assessed the expression of these two genes in synovial organoids. Compared to uninfected organoids, ST80 Δ edinB induced an increase in the expression of *CXCL8* and *PTGS2*, in contrast to the EDIN-B-expressing ST80 WT strain, which was consistent with YAP transcriptional activity inhibition in HEK293 cells.

In conclusion, this organoid-based model confirmed the strong ability of the EDIN-B-expressing ST80 WT strain to inhibit YAP transcriptional activity and reduce the expression of inflammatory mediators. These results suggest that YAP inhibition by EDIN-B can reduce synovial inflammation and prevent immune cell recruitment at the infection site.

Discussion

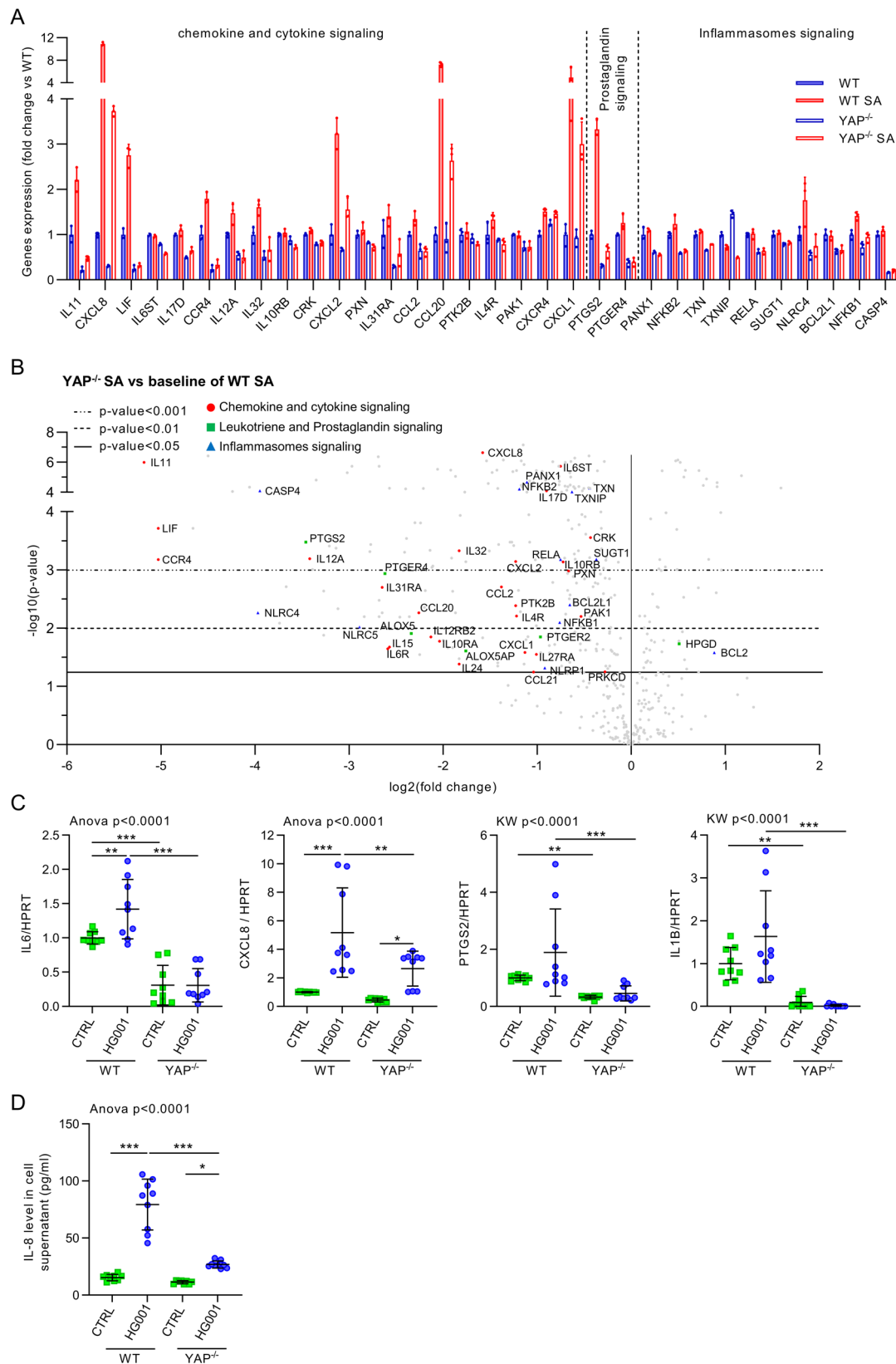
In this study, we sought to investigate whether YAP is involved in the clearance of intracellular *S. aureus*. We demonstrated that YAP plays a critical role in efficient cell-autonomous immune response against intracellular *S. aureus* by controlling autophagy-lysosome and inflammation-related signaling pathways. Moreover, we found that *S. aureus* expressing EDIN-B inhibits the YAP-mediated cell-autonomous immune response. These findings are summarized in Fig. 8.

Our results are consistent with the role of YAP/TAZ transcriptional activity in promoting autophagy^{14,15,52}. In our model of YAP-mutated cells, we found no differences in *MLC2* and *DIAPH1* expression, which is important for autophagosome formation¹⁴. In contrast, we observed alterations in the late phase of autophagy, which is consistent with a previous study showing impaired fusion between autophagosomes and lysosomes¹⁵, but the mechanism involved seems to be different. Indeed, we observed abnormal and oversized autophagolysosomes vesicles. In particular, we found that YAP^{-/-} cells have an alteration in lysosomal acidification, which could be explained by the decreased expression of *ATP6VOD1*, which encodes a V-ATPase subunit required for lysosomal acidification⁵³. Moreover, abnormal and oversized autophagolysosomes with poor degradative functionality have been described in cells deficient for V-ATPase subunits³⁹, which supports

our findings. In addition, we found that *CTSL* was downregulated in the YAP^{-/-} HEK293 cells. It has been shown that *CTSL*-deleted cells have important lysosomal dysfunction and LC3-II accumulation, reflecting an altered autophagic flux³⁸. In addition, we showed that this effect was mediated by the YAP TEAD-binding domain, since YAP Δ TEAD^{-/-} cells display autophagic defects similar to those of YAP^{-/-} cells. However, we cannot exclude the possibility that YAP interacts through its TEAD-binding domain with another transcription factor involved in autophagy and lysosome signaling pathways. Indeed, a recent study showed that YAP can interact with transcription factor EB (TFEB) to induce the expression of autophagic and lysosomal genes⁵² but whether the TEAD-binding domain of YAP is required for its interaction with TFEB is unknown. Thus, YAP-TEAD and/or YAP/TFEB could act synergistically for autophagy- and lysosome-related gene regulation. Overall, our data reinforce the role of YAP in autophagy regulation and provide further insights into how YAP promotes autophagic flux.

Our work shows that YAP transcriptional activity is required to control the replication of *S. aureus*, and that some EDIN-B-expressing *S. aureus* strains can inhibit YAP to promote their own intracellular replication. Given that autophagy is clearly established as a major mechanism for clearing *S. aureus* in vitro and in vivo^{31–33}, the autophagy and lysosomal dysfunction observed in YAP-mutated cells in this study explains why *S. aureus* infection was more pronounced when YAP transcriptional activity was inhibited or absent. Several other studies agree with our results regarding the importance of lysosomal genes for tackling intracellular *S. aureus*^{54,55}. Indeed, *CTSL*-deficient macrophages exhibit a poor ability to remove intracellular *S. aureus*⁵⁴, and genetic manipulations of V-ATPases or bafilomycinA1 treatment in macrophages promoted *S. aureus* intracellular replication⁵⁵, consistent with our results showing increased *S. aureus* replication in CQ-treated HEK293 WT cells. However, to avoid degradation, *S. aureus* has also been found to inhibit the fusion of autophagosomes with lysosomes and escape from autophagic vesicles to replicate inside the cytosol³¹. In our model, the loss of YAP transcriptional activity, which induces the blockage of autophagic flux, was found to promote autophagosome and autophagolysosome escape and replication of *S. aureus*.

In addition, we found that EDIN-B-expressing *S. aureus* inhibited YAP transcriptional activity, which enabled them to replicate more efficiently in the cells, likely by escaping from autophagic vesicles. Autophagy is a conserved cellular process known to be involved in the clearance of intracellular bacteria⁵⁶, and RhoA-targeting toxins (such as EDINs) can be expressed by other pathogenic bacteria such as *Yersinia* and *Salmonella* species^{24,25}. In addition, bacteria secreting RhoA-targeting toxins were found to alter actin dynamics, leading to the impairment of tight and adherent junctions and an increase in bacterial invasion across the epithelium and endothelium^{25,27}. Interestingly, YAP is known to promote the formation of focal adhesion complex, and regulate actin dynamics, and is activated after intestinal barrier disruption following bacterial infection^{14,21,57}. Thus, we speculated that some known RhoA inhibition mechanisms achieved by bacteria could



be mediated by YAP activity. In line with a potential conserved YAP/TAZ antibacterial effect, LegK7 (a *Legionella pneumophila* effector protein) reportedly mimics the effect of MST1 kinase (a key member of the Hippo pathway) leading to YAP/TAZ degradation^{58,59}. Hence, different bacterial toxins can target different YAP/TAZ upstream modulators to achieve YAP/TAZ inhibition, thus, reinforcing that the YAP/

TAZ antibacterial mechanism described in the current study could be applied for other intracellular bacteria.

Increasing evidence demonstrates that YAP-TEAD transcriptional activity can play a pro-inflammatory role by promoting the expression of pro-inflammatory mediators such as *IL6*¹², *CCL2*^{60,61}, *IL8*⁹, *IL1B*¹³, *PTGS2*⁶², and NF- κ B family members⁶³. However, contradictory results

Fig. 6 | YAP promotes inflammatory response during *Staphylococcus aureus* infection.

HEK293 cells were cultured and infected, as described in Fig. 3. **A** nCounter NanoString host response inflammatory gene expression in the four groups; depicted genes were selected if at least one comparison between two groups gave a corrected p value <0.01 , and they must be related to chemokine, cytokine, prostaglandin, or inflammasome signaling as indicated ($n = 3/\text{group}$). **B** Volcano plot representation of differential gene expression in YAP^{-/-} infected group versus the baseline of WT infected group; depicted genes are chemokine and cytokine (red circle), leukotriene and prostaglandin (green square), and

inflammasome (blue triangle) pathway genes differentially expressed. **C** RT-qPCR quantification of *IL6*, *CXCL8*, *PTGS2*, and *IL1B* expression normalized to *HPRT* expression ($n = 9/\text{group}$). **D** IL-8 level in cell supernatant (pg/mL) assessed by ELISA ($n = 9/\text{group}$). Results are expressed as fold change vs. control group (only in **A**, **C**) and presented as histograms (**A**) or individual values (**C**, **D**) with mean \pm SD, representing three independent experiments (**C**, **D**). WT wild-type, SA *S. aureus*. One-way analysis of variance (ANOVA) test with false discovery rate (FDR) correction for multiple comparisons post hoc tests: * $p < 0.05$; ** $p < 0.01$; *** $p < 0.001$.

exist in the literature, indicating an anti-inflammatory role of YAP in mouse models^{20,64,65}. In our study, YAP transcriptional activity was found to have a pro-inflammatory effect in HEK293 cells. We found that the loss of YAP activity decreased the expression of several pro-inflammatory genes known to foster *S. aureus* clearance in vivo. Thus, RhoA-mediated inhibition of YAP by bacteria could be a way to evade the immune system by decreasing the inflammatory response.

Another important question is how bacteria modulate YAP activity in host cells. In contrast to our results, *S. aureus* infection in *Drosophila* was found to increase Yorkie cytoplasmic localization in fly fat bodies²². Yorkie overexpression in fly fat bodies was found to increase *S. aureus*-induced death compared to WT flies²². However, there are important differences between human NPPCs and fly fat bodies, which can influence YAP activity and its subcellular localization upon infection. In mice, several other bacterial species (e.g., *Streptococcus pneumoniae* and *Helicobacter pylori*) lead to nuclear translocation^{18,20}. Thus, it could be interesting to test whether YAP has an anti-*S. aureus* function in mouse models. Although bacteria-induced tissue damage can promote YAP activation in mouse models, the mechanisms that induce nuclear translocation of YAP upon bacterial infection are not fully understood^{20,21}. Our results showed that *S. aureus* supernatant alone is not sufficient to induce YAP nuclear translocation, which suggests that internalization of *S. aureus* is needed for inducing nuclear translocation of YAP. Interestingly, *S. aureus* internalization is mainly driven by $\alpha 5\beta 1$ integrins, which trigger the activation of focal adhesion kinase (FAK)³⁰. YAP is known to be highly sensitive to cell mechanical stimulation, such as integrin-FAK activation, which increases RhoA activity and causes YAP nuclear translocation⁶⁶. Thus, it will be important to investigate whether YAP activation following *S. aureus* internalization could be a nonspecific “danger signal” by converting cell mechanical events into cell-autonomous immune responses, including xenophagy and inflammatory responses.

Overall, this work provides key fundamental insights into the role of YAP in cell-autonomous immune responses. It also provides further insights into the role of the C3 exoenzyme EDIN during *S. aureus* infections. Thus, the findings of this work could help find more effective ways to fight intracellular bacteria and pave the way for future microbiology and YAP-related investigations.

Methods

Cell culture

HEK293 cells were cultured in Dulbecco’s modified Eagle’s medium (DMEM, Sigma-Aldrich, St. Louis, MO, USA) with 10% fetal bovine serum (FBS), 1% non-essential amino acid solution, and 1% penicillin and streptomycin (PS) solution. The plates were coated with fibronectin (1:100, Sigma-Aldrich, F1141) for 2 h at 37 °C before use. HEK293 cells were grown at different cell densities: For low density (LD) cell culture, cells were seeded at 10,000 cells/cm² and used 24 h after seeding; for medium density (MD) cell culture, cells were seeded at 100,000 cells/cm² and used 24 h after seeding; for high density (HD) cell culture, cells were seeded at 100,000 cells/cm² and used 72 h after seeding.

Cell line generation using CRISPR-Cas9 technology

HEK293 YAP^{-/-} were generated using commercially available plasmids with specific CRISPR-Cas-9 single guide RNA (sgRNA) and sequence for

homology-directed repair targeting YAP sequence (Santa Cruz Biotechnology, Dallas, TX, USA) as previously reported³⁶. HEK293 YAP Δ -TEAD^{+/+} cells were generated using the CRISPR-Cas9 technique and homology-directed repair. sgRNA was designed to cut in exon 1 of the YAP gene at proline 98 using the following protospacer: 5'-CGAC TCCTTCTCAAGCCGC-3'. Homologous recombination was supported by a donor plasmid with a 5' homology arm of 681 bp, a 3' homology arm of 837 + 12 bp, whose original sequence TTCAAGCCGCCG was modified by the sequence AGAAGAAGAAGA that introduced the following mutations: Phe96Arg, Lys97Arg, Pro98Arg, and Pro99Arg. CRISPR-Cas9 and donor plasmids were manufactured on demand by VectorBuilder (VectorBuilder, Neu-Isenburg, Germany). HEK293 cells were transfected with 0.5 μ g of each plasmid and 2 μ L transfection reagent (Jet prime, Polyplus transfection, New York, NY, USA) in a final volume of 100 μ L. After 48 h of transfection, the cells were seeded at one cell per well in a 96-well plate for monoclonal expansion. Mutations following homologous recombination were confirmed by PCR sequencing (Eurofins Genomics, Nantes, France).

Bacterial strains and plasmids

Staphylococcus aureus strains used in the study were the HG001 strain, which is a methicillin-susceptible *S. aureus* (MSSA) strain that lacks *edin* genes⁶⁷ and the LUG1799 strain, which is a minimally passaged strain belonging to the European lineage community-acquired methicillin-resistant *S. aureus* (CA-MRSA) ST80-MRSA-IV strain⁶⁸ and is referred to as ST80 wild-type (WT) and its isogenic *edinB* mutant that is referred to as ST80 Δ *edinB*²⁷. All strains were stored at -20 °C in cryotubes.

For live-cell imaging, the plasmid pSK265, a derivative of pC194⁶⁹, was used to express the *DsRed* gene under the control of the *rpob* promoter in *S. aureus* strains. All strains were transformed with the plasmid pSK265::DsRed by electroporation (Gene Pulser, Bio-Rad) and were grown at 37 °C on blood agar (43049, Biomérieux) or tryptic soy agar (TSA) (920241, Becton Dickinson) supplemented with 20 μ g/mL of chloramphenicol when appropriate.

Organoid culture and processing

Synovial organoids were assembled as previously described⁷⁰ with modifications³⁶. Fibroblast-like synoviocytes (FLS) were collected from osteoarthritis (OA) patients who provided written consent after oral information (IRB # 2014-A01688-39). FLS were mixed in phenol red-free Matrigel (356237, Corning, Corning, NY, USA) at 4×10^6 cells/mL, and a single 22 μ L droplet (representing approximately 90,000 cells) was added to each well of a 96-well U-shaped very low-attachment surface plate (CLS4515, Corning). The plate was incubated at 37 °C in 5% CO₂ for 45 min to allow droplet gelation. Wells containing solidified droplets were filled with 200 μ L of DMEM high-glucose medium supplemented with 10% FBS, 1% glutamine, 1% non-essential amino acids, 1% PS, 0.1 mM ascorbic acid, and insulin (10 μ g/mL)-transferrin (10 μ g/mL)-selenium (3×10^{-8} M) solution at 37 °C in 5% CO₂ for 21 days. At day 21, organoids were fixed with glyoxal solution at pH 4.5 (e.g., for 500 mL: 355 mL ddH₂O, 99 mL ethanol, 39 mL glyoxal (128465, Sigma-Aldrich), and 1 mL acetic acid) for 1 h at room temperature (RT) because PFA fixation was deleterious. Organoids were embedded in a gelatin 100 G (7.5%)-sucrose (10%) solution and frozen in an isopentane bath at -50 °C for 2 min before storage at -80 °C.

Fig. 7 | *Staphylococcus aureus* EDIN-B expression decreased YAP activity in a synovial organoid model. Primary fibroblast-like synoviocytes (FLSs) from human osteoarthritic patients ($n = 3$) were used to form synovial organoids. Organoids were infected with 1×10^8 *S. aureus* per mL. *S. aureus* ST80 strains were allowed to contact organoids for 30 min and imaged immediately (A) or let in contact for 2 h upon agitation, then, lysostaphin was added at 10 μ g/mL for the rest of the experiments to avoid extracellular *S. aureus* multiplication. **A** Confocal z-stack max intensity projection images of live organoids labeled with SiR-actin (actin filaments, magenta); DsRed-expressing *S. aureus* (red); images were obtained from the surface of the organoid and are representative of three independent experiments; scale bar: 25 μ m. **B, C** Confocal representative z-stack maximum intensity projection of 30 μ m thick cryosections of the entire organoid (**B**) or the lining layer (**C**); # organoid stromal part, *outside of the organoid, dotted line: limit between lining layer and stromal part, white arrow: local synovial thickening; Scale bar: 200 μ m (**B**),

25 μ m (**C**). **D** Microscopy quantification of synovial lining layer thickness (CTRL $n = 14$, ST80 WT $n = 15$, ST80 Δ edinB $n = 15$). **E** Confocal representative z-stack max intensity projection images of 30 μ m thick cryosections labeled with anti-YAP antibody (green), DAPI (nuclei, blue) and phalloidin (actin filaments, magenta); DsRed-expressing *S. aureus* (red); scale bar: 20 μ m or 5 μ m for zoom. **F** RT-qPCR quantification of *CTGF*, *CYR61*, *CXCL8*, and *PTGS2* expression normalized to *HPRT* expression (n : sample/group). Results are expressed as fold change vs. control group and presented as individual values with mean \pm SD, and representative of three independent experiments corresponding to three different fibroblast-like synoviocytes (FLS) donors. WT wild-type, ST80 Δ edinB: EDIN-B-deleted ST80 strain. One-way analysis of variance (ANOVA) or Kruskal-Wallis (KW) test with false discovery rate (FDR) correction for multiple comparisons post hoc tests: * $p < 0.05$; ** $p < 0.01$; *** $p < 0.001$.

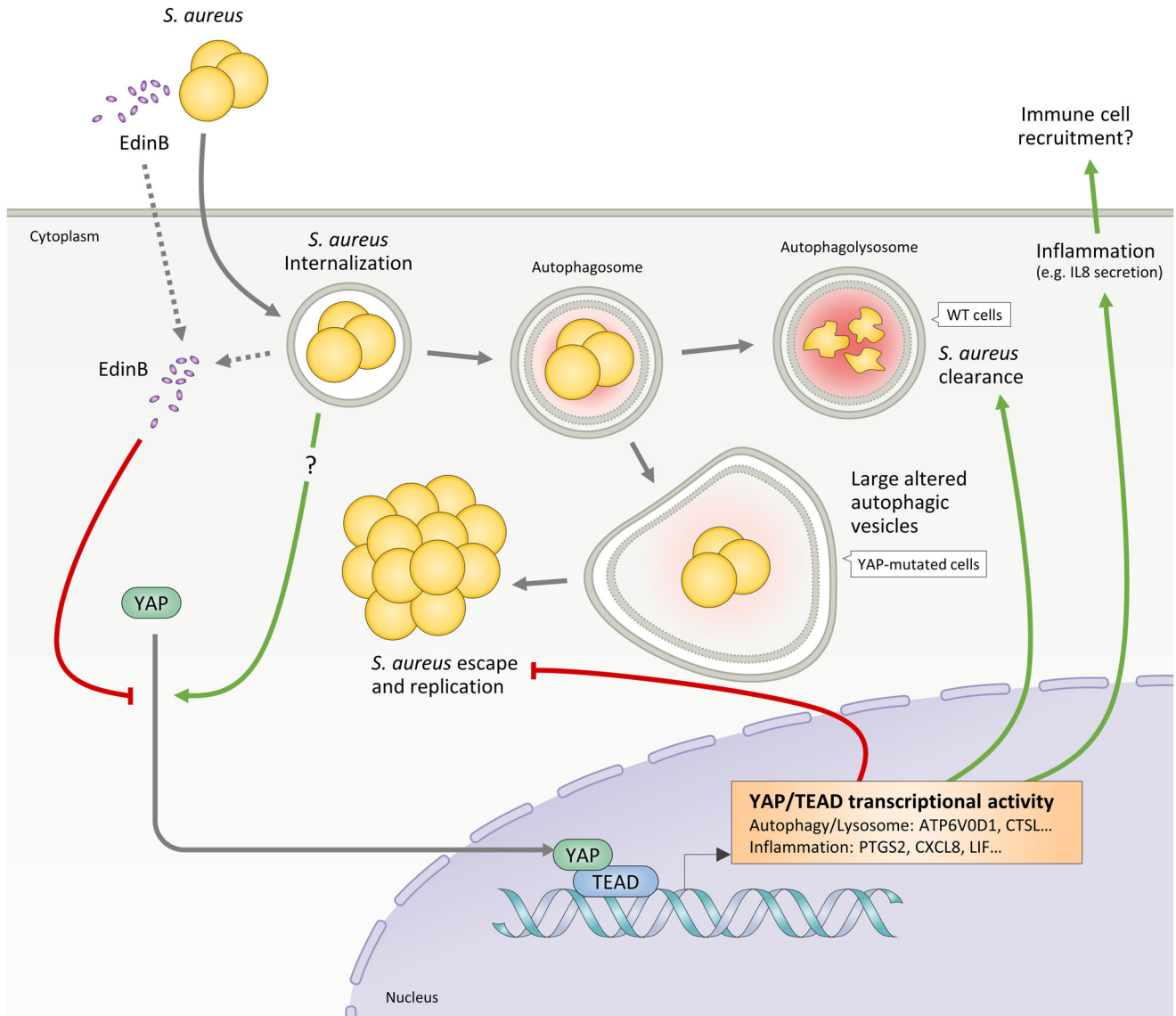


Fig. 8 | Model of the YAP-mediated cell-autonomous immune response against intracellular *S. aureus*. After *S. aureus* internalization by the host cell, YAP is translocated to the nucleus and promotes the expression of host genes involved in cell-autonomous immune response, including genes involved in autophagy, lysosome activity and inflammatory response. In WT cells, autophagic machinery limit intracellular replication of *S. aureus*. In contrast, YAP-mutated cells, which have

large altered autophagic vesicles, exhibit a lower efficiency in limiting intracellular replication of *S. aureus*. *edinB*-positive *S. aureus* strain secretes the C3 exoenzyme-like toxin EDIN-B that inhibit YAP-mediated cell-autonomous immune response. WT wild-type, YAP Yes-associated protein, TEAD TEA domain transcription factor, EDIN-B epidermal cell differentiation inhibitor-B.

seeded on agar plates and quantified after a 24-h incubation period to verify the real bacterial concentration. To quantify the intracellular load of *S. aureus* by culture, HEK293 cells were washed with phosphate buffered saline (PBS) to remove lysostaphin. Cells were lysed by osmotic shock using lysis buffer containing 0.25% Triton X-100 (Sigma-Aldrich), 0.25X trypsin-EDTA (Sigma-Aldrich), and sterile water. The *S. aureus* load of cell lysates was quantified on an agar plate using an automatic plate seeder (EasySpiral Dilute, Interscience, St-Nom la Bretèche, France) and a colony counter (Scan 4000, Interscience).

Immunofluorescence

HEK293 cells were fixed with 4% PFA at RT for 20 min (for YAP immunolabeling) or in ice-cold methanol for 15 min (for LC3A/B immunolabeling). Fixed and frozen organoids were cryosectioned to a thickness of 30 μm . Samples (cells or cryosections) were rehydrated in PBS for 10 min and permeabilized in 0.3% Triton X-100 for 15 min. The samples were then incubated in blocking buffer containing 1% BSA, 5% goat serum, and 0.1% Triton-X-100 for 60 min at RT. Subsequently, the samples were incubated with the primary antibody or isotypic control diluted in blocking buffer overnight at 4 °C. The antibodies used were mouse IgG anti-YAP antibody (63.7 sc-101199, Santa Cruz Biotechnology; 1:100), rabbit anti-LC3A/B antibody (4108, Cell Signaling Technology, Leiden, The Netherlands; 1/100), mouse and rabbit IgG isotype antibody (31903 and 31235, Thermo Fisher Scientific; used at the same concentration as YAP or LC3A/B antibodies). After washing, the cells were incubated with secondary antibody, goat anti-mouse 488 or goat anti-rabbit 488 diluted in blocking buffer (A11034 and A32731, Thermo Fisher; 1:400) for 75 min at RT. The cells were counterstained with 4',6-diamidino-2-phenylindole (DAPI) for 10 min at 37 °C with or without dye-labeled phalloidin (ab176753 or ab176759, Abcam, Cambridge, UK) for 1 h at 37 °C.

Live-cell confocal microscopy of HEK293 cells or organoids

Cells and organoids were uninfected or infected with DsRed-expressing *S. aureus* strains using the EPA technique described above. Additionally, cell permeable C3 exoenzyme from *C. botulinum* (CT04, Cytoskeleton, Denver, CO, USA) was used at 1 $\mu\text{g}/\text{mL}$, while CQ was used at 50 μM to treat cells. In HEK293 cells, autophagosomes were labeled using the CYTO-ID Autophagy Detection Kit 2.0 (ENZ-KIT175, Enzo Life Sciences) as recommended by the manufacturer. Briefly, 30 min before image recording (*i.e.*, 2.5 hpi or 6.5 hpi), the media was discarded, and cells were washed once with the CYTO-ID assay buffer. Cells were incubated with a staining solution comprising the CYTO-ID Green detection reagent (1:500) and 5 $\mu\text{g}/\text{mL}$ Hoechst 33342 in CYTO-ID assay buffer for 30 min at 37 °C and 5% CO₂ protected from light. Optionally, SiR-Lysosome (CY-SC012, Cytoskeleton) was added at 1 μM in the staining solution to label lysosomes. Cells were then washed once with the CYTO-ID assay buffer and imaged immediately by confocal microscopy at 3 hpi and 7 hpi. Of note, the microscopy slides were discarded after imaging, thus 3 hpi and 7 hpi conditions were recorded on different slides.

In organoids, F-Actin was labeled with SiR-Actin dye (1:5000, Cytoskeleton) for 4 h prior to infection.

Image acquisition and quantification

Images were acquired using a spinning disk confocal microscope (Ti2 CSU-W1, Nikon, France) with a 60x objective (CFI Plan Apo Lambda S 60x/1.40, MRD1605, Nikon) or using a confocal laser scanning microscope (CLSM) (LSM 800 airyscan, Zeiss, Oberkochen, Germany) with a 10x objective (Plan-Apochromat 10x/0.45 M27, Zeiss). Image analysis was performed with the General Analysis 3 module of the NIS software (v5.30, Nikon) or Fiji software (v1.52p, NIH, USA).

In HEK293 cells, YAP immunolabeling was quantified using an automatic macro developed with the NIS software to measure MFI in the cytoplasmic and nuclear areas and to calculate the NC ratio by

dividing the nuclear MFI by the cytoplasmic MFI. CYTO-ID and SiR-Lysosome quantification was also performed using the NIS software. Briefly, the images were denoised and binarized in 3D. The CYTO-ID vesicle count and volume as well as the *S. aureus* volume were measured, and the colocalization between the *S. aureus* volume and CYTO-ID vesicle volume was assessed. The same was performed for SiR-Lysosome labeling, use to assess the colocalization between SiR-Lysosome and *S. aureus* or between SiR-Lysosome, CYTO-ID, and *S. aureus*. The cell area was determined using an extended area of Hoechst labeling. For each cell, the count and mean volume of the CYTO-ID and SiR-Lysosome vesicles were measured. The same method was used to measure the *S. aureus* volume per cell. Quantifications were performed by analyzing 2 to 5 fields per well using a 60x objective.

For organoid lining layer thickness, quantification was performed with the Fiji software using cryosections stained with DAPI and dye-labeled phalloidin. Two slices per organoid were assessed. Quantification was performed on tile images acquired with a 10x objective, allowing quantification of the entire structure. Images were binarized, and the synovial lining layer area was automatically selected. The organoid perimeter was then measured. The lining layer thickness was the result of the synovial lining layer area divided by the perimeter of the synovial organoid.

Luciferase assay

HEK293 cells were transfected in 96-well plates with the 8xGTIIc-luciferase plasmid (firefly luciferase, # 34615, Addgene, Watertown, MA, US) and the pRL-SV40P plasmid (Renilla luciferase, # 27163, Addgene), using 0.5 μg of each plasmid and 2 μL of the jetPRIME transfection reagent (Polyplus transfection, New York, NY, USA) in a final volume of 100 μL per well and incubated overnight at 37 °C in 5% CO₂. The next day, the spent medium was replaced with the fresh complete culture medium, and the cells were incubated for another 24 h at 37 °C in 5% CO₂. The day after, the transfected cells were challenged with *S. aureus* or supernatant only, as mentioned in the text. After the challenge, the cells were lysed and luminescence was quantified using the Promega dual glow assay (Promega, Madison, WI, USA) with a multimodal plate reader (TriStar, Berthold). The blank value was subtracted, and the firefly luciferase activity was divided by the Renilla luciferase activity to normalize the results according to the number of cells.

Protein extraction and western blotting

HEK293 cells were uninfected or infected with HG001 *S. aureus* strain using the EPA technique described above. Cells were treated with CQ (50 μM) for 24 h, and rapamycin (500 nM) for 24 h. Protein extraction was performed using the Allprep RNA/Protein Kit (80404 Qiagen Inc., Hilden, Germany). For YAP/TAZ labeling, proteins (10–20 μg) were denatured and separated for 20 min at 200 V on 8% Bis-Tris gels (NW00082BOX, Thermo Fisher Scientific) before being transferred onto the polyvinylidene difluoride membrane (IB24002, Thermo Fisher Scientific). For LC3 labeling, proteins (10–20 μg) were denatured and separated for 25 min at 220 V and 4 °C on 16% Tris-Glycine gels (XP00162BOX, Thermo Fisher Scientific) before being transferred onto the polyvinylidene difluoride membrane (IB24002, Thermo Fisher Scientific). The membranes were blocked in TBS Tween 0.1% with 5% skimmed milk and incubated with primary antibody overnight at 4 °C. Primary antibodies purchased from Cell Signaling Technology (Danvers, MA, USA) were diluted at 1:1,000: YAP/TAZ (#8418), YAP (#14074), LC3A/B (#12741), and 1:5,000: GAPDH (#2118). The membrane was washed with TBS Tween 0.1% and incubated with a horseradish peroxidase-conjugated secondary antibody (31460, Thermo Fisher Scientific; 1:5000) for 1 h at RT. Immunoreactive protein bands were revealed using the Clarity Western ECL Substrate (Bio-Rad, Hercules, CA, USA) and images were recorded using CDD cooled camera

(ibright FL1500 imaging system, Thermo Fisher Scientific). Quantification was performed using the gel analyzer function of Fiji software (v1.52p, NIH, USA).

RNA extraction and RT-qPCR

For synovial organoids, lysis was performed using the TRI Reagent (Sigma-Aldrich); three synovial organoids were pooled together during the lysis step to yield sufficient RNA.

For synovial organoids, the aqueous phase was processed following lysis in the TRI Reagent for RNA extraction and purification. For cell culture, RNA was extracted using the Allprep RNA/Protein Kit (Qiagen). The quality and quantity of RNA were assessed using the Experion RNA Analysis Kit (Bio-Rad) and QuantIT RiboGreen RNA Assay Kit (Thermo Fisher Scientific), respectively. Complementary DNA (cDNA) was synthesized using an iScript cDNA Synthesis Kit (Bio-Rad). Quantitative RT polymerase chain reaction (PCR) was performed using the CFX96 RealTime System (Bio-Rad) with LightCycler FastStart DNA Master plus SYBR Green I (Roche Diagnostics, Basel, Switzerland). The results were normalized to the housekeeping gene expression hypoxanthine-guanine phosphoribosyltransferase (HPRT). The sequences of the primers used in this study are available upon request.

Measure of lysosomal acidification kinetic

Cells were seeded in 96-well plates (CELLSTAR μ Clear 96-well ref 655090, Greiner Bio-One, Courtaboeuf, France) at a density of 100,000 cells/cm² and incubated for 24 h at 37 °C with 5% CO₂. Subsequently, cells were incubated with Bafilomycin A1 for 2 h to increase the lysosomal pH, and then washed with PBS. The lysosensor yellow/blue DND-160 probe (L7545, Thermo Fisher Scientific) was added to the cells, according to the manufacturer's instructions, and fluorescence intensities at $\lambda_{ex/em}$ 405/450 and 405/550 nm were immediately recorded using a multimodal plate reader (Infinity 200, Tecan, Lyon, France). After 20 min of incubation with the lysosensor probe, fluorescence intensities at $\lambda_{ex/em}$ 405/450 and 405/550 nm were recorded again to assess the kinetic of lysosomal acidification.

Quantification of IL-8 secretion

HEK293 WT or YAP^{-/-} cells were uninfected or infected with the *S. aureus* HG001 strain using the EPA technique described above. Supernatant was collected at 7 hpi and the associated IL-8 levels were measured using an ELISA kit (#88-8086, Thermo Fisher Scientific, Waltham, MA, USA) according to the manufacturer's recommendations.

Transcriptomic analysis using nCounter Host Response Panel

The nCounter Host Response panel (Nanostring technology), which includes 770 genes involved in host response processes, was performed with the nCounter Sprint instrument following the manufacturer's recommendations. Briefly, we used 50 ng of RNA extracted from WT or YAP^{-/-} HEK293 infected (or not) with the HG001 strain at MOI 10 for 7 h ($n=3$ per group). All quality controls were performed according to the manufacturer's instructions. Normalization was performed using the housekeeping genes identified by the geNorm analysis using the NanoString advance software. The count detection limit was determined using a threshold based on the negative controls. Data analysis was performed using the nSolver package (version 3.0) and the Advanced Analysis module (version 1.0.36). Differential expression and pathway analyses were performed using the nSolver advance analysis module according to the guidance given by manufacturer's instructions. Genes with a false discovery rate (FDR)-corrected p value <0.05 were considered significantly differentially expressed.

Statistical analysis

Data are represented as single values with mean and standard deviation and are expressed, if indicated in the figure legend, as a fold change of the mean of control values. The results are representative of

at least three independent experiments. Unpaired T-test was used to compare two groups. Multiple comparisons were performed by one-way analysis of variance (ANOVA) or Kruskal-Wallis test, and post hoc comparisons were corrected using the FDR method of Benjamini and Hochberg. Results were considered significantly different when $p < 0.05$ or $q < 0.05$. All statistical analyses were performed using the GraphPad software (v9.3.0, Prism). The NanoString results were analyzed using the nSolver software (v4.0, NanoString Technology) and nSolver Advance Analysis Module (v2.0.134, NanoString Technology).

Reporting summary

Further information on research design is available in the Nature Research Reporting Summary linked to this article.

Data availability

The data generated in this study are provided in the Source Data file. The Nanostring nCounter data generated in this study have been deposited in the Gene Expression Omnibus (GEO) database under accession code [GSE197181](https://www.ncbi.nlm.nih.gov/geo/query/acc.cgi?acc=GSE197181). Source data are provided with this paper.

References

- Dong, J. et al. Elucidation of a Universal Size-Control Mechanism in *Drosophila* and Mammals. *Cell* **130**, 1120–1133 (2007).
- Vassilev, A., Kaneko, K. J., Shu, H., Zhao, Y. & DePamphilis, M. L. TEAD/TEF transcription factors utilize the activation domain of YAP65, a Src/Yes-associated protein localized in the cytoplasm. *Genes Dev.* **15**, 1229–1241 (2001).
- Hilman, D. & Gat, U. The Evolutionary History of YAP and the Hippo/YAP Pathway. *Mol. Biol. Evolution* **28**, 2403–2417 (2011).
- Li, Z. et al. Structural insights into the YAP and TEAD complex. *Genes Dev.* **24**, 235–240 (2010).
- Liu, C.-Y. et al. The Hippo Tumor Pathway Promotes TAZ Degradation by Phosphorylating a Phosphodegron and Recruiting the SCF β -TrCP E3 Ligase. *J. Biol. Chem.* **285**, 37159–37169 (2010).
- Zhao, B. et al. Inactivation of YAP oncoprotein by the Hippo pathway is involved in cell contact inhibition and tissue growth control. *Genes Dev.* **21**, 2747–2761 (2007).
- Dupont, S. et al. Role of YAP/TAZ in mechanotransduction. *Nature* **474**, 179–183 (2011).
- Aragona, M. et al. A Mechanical Checkpoint Controls Multicellular Growth through YAP/TAZ Regulation by Actin-Processing Factors. *Cell* **154**, 1047–1059 (2013).
- Wang, L. et al. Integrin-YAP/TAZ-JNK cascade mediates atheroprotective effect of unidirectional shear flow. *Nature* **540**, 579–582 (2016).
- Zanconato, F., Cordenonsi, M. & Piccolo, S. YAP/TAZ at the Roots of Cancer. *Cancer Cell* **29**, 783–803 (2016).
- Geng, J. et al. The transcriptional coactivator TAZ regulates reciprocal differentiation of TH17 cells and Treg cells. *Nat. Immunol.* **18**, 800–812 (2017).
- Taniguchi, K. et al. A gp130–Src–YAP module links inflammation to epithelial regeneration. *Nature* **519**, 57–62 (2015).
- Zhou, X. et al. YAP Aggravates Inflammatory Bowel Disease by Regulating M1/M2 Macrophage Polarization and Gut Microbial Homeostasis. *Cell Rep.* **27**, 1176–1189.e5 (2019).
- Pavel, M. et al. Contact inhibition controls cell survival and proliferation via YAP/TAZ-autophagy axis. *Nat. Commun.* **9**, 2961 (2018).
- Totaro, A. et al. Cell phenotypic plasticity requires autophagic flux driven by YAP/TAZ mechanotransduction. *Proc. Natl Acad. Sci. U.S.A.* **116**, 17848–17857 (2019).
- Krausgruber, T. et al. Structural cells are key regulators of organ-specific immune response. *Nature* **583**, 296–302 (2020).
- Randow, F., MacMicking, J. D. & James, L. C. Cellular Self-Defense: How Cell-Autonomous Immunity Protects Against Pathogens. *Science* **340**, 701–706 (2013).

18. Wu, Y. et al. Helicobacter pylori-induced YAP1 nuclear translocation promotes gastric carcinogenesis by enhancing IL-1 β expression. *Cancer Med* **8**, 3965–3980 (2019).
19. García-Gil, A. et al. SopB activates the Akt-YAP pathway to promote Salmonella survival within B cells. *Virulence* **9**, 1390–1402 (2018).
20. LaCanna, R. et al. Yap/Taz regulate alveolar regeneration and resolution of lung inflammation. *J. Clin. Invest* **129**, 2107–2122 (2019).
21. Ma, Y.-C. et al. YAP in epithelium senses gut barrier loss to deploy defenses against pathogens. *PLOS Pathog.* **16**, e1008766 (2020).
22. Liu, B. et al. Toll Receptor-Mediated Hippo Signaling Controls Innate Immunity in Drosophila. *Cell* **164**, 406–419 (2016).
23. Sugai, M., Chen, C. H. & Wu, H. C. Bacterial ADP-ribosyltransferase with a substrate specificity of the rho protein disassembles the Golgi apparatus in Vero cells and mimics the action of brefeldin A. *PNAS* **89**, 8903–8907 (1992).
24. Aktories, K. Bacterial protein toxins that modify host regulatory GTPases. *Nat. Rev. Microbiol* **9**, 487–498 (2011).
25. Lemichez, E. & Aktories, K. Hijacking of Rho GTPases during bacterial infection. *Exp. Cell Res* **319**, 2329–2336 (2013).
26. Munro, P. et al. The *Staphylococcus aureus* epidermal cell differentiation inhibitor toxin promotes formation of infection foci in a mouse model of bacteremia. *Infect. Immun.* **78**, 3404–3411 (2010).
27. Courjon, J. et al. EDIN-B Promotes the Translocation of *Staphylococcus aureus* to the Bloodstream in the Course of Pneumonia. *Toxins* **7**, 4131–4142 (2015).
28. Munro, P. et al. High prevalence of edin-C encoding RhoA-targeting toxin in clinical isolates of *Staphylococcus aureus*. *Eur. J. Clin. Microbiol Infect. Dis.* **30**, 965–972 (2011).
29. Tong, S. Y. C., Davis, J. S., Eichenberger, E., Holland, T. L. & Fowler, V. G. *Staphylococcus aureus* Infections: Epidemiology, Pathophysiology, Clinical Manifestations, and Management. *Clin. Microbiol. Rev.* **28**, 603–661 (2015).
30. Josse, J., Laurent, F. & Diot, A. Staphylococcal Adhesion and Host Cell Invasion: Fibronectin-Binding and Other Mechanisms. *Front. Microbiol.* **8**, 2433 (2017).
31. Neumann, Y. et al. Intracellular *Staphylococcus aureus* eludes selective autophagy by activating a host cell kinase. *Autophagy* **12**, 2069–2084 (2016).
32. Gibson, J. F. et al. Neutrophils use selective autophagy receptor Sqstm1/p62 to target *Staphylococcus aureus* for degradation in vivo in zebrafish. *Autophagy* **17**, 1448–1457 (2021).
33. Maurer, K. et al. Autophagy Mediates Tolerance to *Staphylococcus aureus* Alpha-Toxin. *Cell Host Microbe* **17**, 429–440 (2015).
34. Rigail, J. et al. Improved Enzyme Protection Assay to Study *Staphylococcus aureus* Internalization and Intracellular Efficacy of Antimicrobial Compounds. *J. Vis. Exp.* **175** (2021).
35. Molinari, G. et al. Localization of the C3-Like ADP-Ribosyltransferase from *Staphylococcus aureus* during Bacterial Invasion of Mammalian Cells. *Infect. Immun.* **74**, 3673–3677 (2006).
36. Caire, R. et al. YAP/TAZ: Key Players for Rheumatoid Arthritis Severity by Driving Fibroblast Like Synoviocytes Phenotype and Fibro-Inflammatory Response. *Front. Immunol.* **12**, 5232 (2021).
37. Hirst, J., Borner, G. H. H., Harbour, M. & Robinson, M. S. The aTiphilin/p200/gamma-synergin complex. *Mol. Biol. Cell* **16**, 2554–2565 (2005).
38. Jung, M., Lee, J., Seo, H.-Y., Lim, J. S. & Kim, E.-K. Cathepsin Inhibition-Induced Lysosomal Dysfunction Enhances Pancreatic Beta-Cell Apoptosis in High Glucose. *PLOS ONE* **10**, e0116972 (2015).
39. Mauvezin, C., Nagy, P., Juhász, G. & Neufeld, T. P. Autophagosome-lysosome fusion is independent of V-ATPase-mediated acidification. *Nat. Commun.* **6**, 7007 (2015).
40. Zanconato, F. et al. Genome-wide association between YAP/TAZ/TEAD and AP-1 at enhancers drives oncogenic growth. *Nat. Cell Biol.* **17**, 1218–1227 (2015).
41. Caire, R. et al. YAP Transcriptional Activity Dictates Cell Response to TNF In Vitro. *Front Immunol.* **13**, 856247 (2022).
42. Baird, G. S., Zacharias, D. A. & Tsien, R. Y. Biochemistry, mutagenesis, and oligomerization of DsRed, a red fluorescent protein from coral. *Proc. Natl Acad. Sci. U.S.A.* **97**, 11984–11989 (2000).
43. West, N. R. Coordination of Immune-Stroma Crosstalk by IL-6 Family Cytokines. *Front. Immunol.* **10**, 1093 (2019).
44. Borish, L. & Rocklin, R. E. Effects of leukocyte inhibitory factor (LIF) on neutrophil phagocytosis and bactericidal activity. *J. Immunol.* **138**, 1475–1479 (1987).
45. Chensue, S. W. Molecular Machinations: Chemokine Signals in Host-Pathogen Interactions. *Clin. Microbiol Rev.* **14**, 821–835 (2001).
46. Reyes-Robles, T. et al. *Staphylococcus aureus* Leukotoxin ED Targets The Chemokine Receptors CXCR1 and CXCR2 to Kill Leukocytes and Promote Infection. *Cell Host Microbe* **14**, 453–459 (2013).
47. Bernard, J. J. & Gallo, R. L. Cyclooxygenase-2 Enhances Anti-microbial Peptide Expression and Killing of *Staphylococcus aureus*. *J. Immunol.* **185**, 6535–6544 (2010).
48. Miller, L. S. et al. MyD88 mediates neutrophil recruitment initiated by IL-1R but not TLR2 activation in immunity against *Staphylococcus aureus*. *Immunity* **24**, 79–91 (2006).
49. Barton, G. M. A calculated response: control of inflammation by the innate immune system. *J. Clin. Investig.* **118**, 413–420 (2008).
50. Roelofs, A. J. et al. Joint morphogenetic cells in the adult mammalian synovium. *Nat. Commun.* **8**, 15040 (2017).
51. Symons, R. A. et al. Targeting the IL-6–Yap–Snail signalling axis in synovial fibroblasts ameliorates inflammatory arthritis. *Ann. Rheum. Dis.* **81**, 214–224 (2022).
52. Ikeda, S. et al. YAP plays a crucial role in the development of cardiomyopathy in lysosomal storage diseases. *J. Clin. Investig.* **131**, 143173 (2021).
53. Xia, Y. et al. The macrophage-specific V-ATPase subunit ATP6VOD2 restricts inflammasome activation and bacterial infection by facilitating autophagosome-lysosome fusion. *Autophagy* **15**, 960–975 (2019).
54. Müller, S. et al. The endolysosomal cysteine cathepsins L and K are involved in macrophage-mediated clearance of *Staphylococcus aureus* and the concomitant cytokine induction. *FASEB J.* **28**, 162–175 (2014).
55. Geng, N. et al. *Staphylococcus aureus* Avoids Autophagy Clearance of Bovine Mammary Epithelial Cells by Impairing Lysosomal Function. *Front. Immunol.* **11**, 746 (2020).
56. Cong, Y., Dinesh Kumar, N., Mauthe, M., Verlhac, P. & Reggiori, F. Manipulation of selective macroautophagy by pathogens at a glance. *J. Cell Sci.* **133**, jcs240440 (2020).
57. Nardone, G. et al. YAP regulates cell mechanics by controlling focal adhesion assembly. *Nat. Commun.* **8**, 15321 (2017).
58. Lee, P.-C. & Machner, M. P. The Legionella Effector Kinase LegK7 Hijacks the Host Hippo Pathway to Promote Infection. *Cell Host Microbe* **24**, 429–438.e6 (2018).
59. Lee, P.-C. et al. The Legionella kinase LegK7 exploits the Hippo pathway scaffold protein MOB1A for allostery and substrate phosphorylation. *Proc. Natl Acad. Sci. U.S.A.* **117**, 14433–14443 (2020).
60. Liu, M. et al. Macrophage K63-Linked Ubiquitination of YAP Promotes Its Nuclear Localization and Exacerbates Atherosclerosis. *Cell Rep.* **32**, 107990 (2020).
61. Kim, W. et al. Hepatic Hippo signaling inhibits pro-tumoral micro-environment to suppress hepatocellular carcinoma. *Gut* **67**, 1692–1703 (2018).
62. Li, W. et al. YAP transcriptionally regulates COX-2 expression and GCCSystm-4 (G-4), a dual YAP/COX-2 inhibitor, overcomes drug

- resistance in colorectal cancer. *J. Exp. Clin. Cancer Res.* **36**, 144 (2017).
63. Wang, Q. et al. REGγ Controls Hippo Signaling and Reciprocal NF-κB–YAP Regulation to Promote Colon Cancer. *Clin. Cancer Res.* **24**, 2015–2025 (2018).
64. Deng, Y. et al. Reciprocal inhibition of YAP/TAZ and NF-κB regulates osteoarthritic cartilage degradation. *Nat. Commun.* **9**, 4564 (2018).
65. Lv, Y. et al. YAP Controls Endothelial Activation and Vascular Inflammation Through TRAF6. *Circ. Res.* **123**, 43–56 (2018).
66. Elbediwy, A. et al. Integrin signalling regulates YAP and TAZ to control skin homeostasis. *Development* **143**, 1674–1687 (2016).
67. Herbert, S. et al. Repair of global regulators in *Staphylococcus aureus* 8325 and comparative analysis with other clinical isolates. *Infect. Immun.* **78**, 2877–2889 (2010).
68. Perret, M. et al. Cross-talk between *Staphylococcus aureus* leukocidins-intoxicated macrophages and lung epithelial cells triggers chemokine secretion in an inflammasome-dependent manner. *Cell Microbiol* **14**, 1019–1036 (2012).
69. Jones, C. L. & Khan, S. A. Nucleotide sequence of the enterotoxin B gene from *Staphylococcus aureus*. *J. Bacteriol.* **166**, 29–33 (1986).
70. Kiener, H. P., Lee, D. M., Agarwal, S. K. & Brenner, M. B. Cadherin-11 Induces Rheumatoid Arthritis Fibroblast-Like Synoviocytes to Form Lining Layers in Vitro. *Am. J. Pathol.* **168**, 1486–1499 (2006).

Acknowledgements

The strain of *Staphylococcus aureus* HG001 was provided by Tarek Msadek (Institut Pasteur, France). The authors acknowledge Eloïse Barrel and Quentin Peyrot for their technical assistance, and all the members of the GIMAP and LBTO teams for their help and feedback. This work was supported by a grant from the FINOVI association (#AO13 FINOVI) under the aegis of the Foundation for the University of Lyon (POV).

Author contributions

R.C., E.A., and P.O.V. designed the experiments. R.C. performed the experiments, designed and performed the CRISPR-cas9 based HEK293 mutation and developed the synovial organoid model. E.A. contributed to the plasmid design for YAPΔTEAD^{-/-} cell generation. M.T. contributed to the nanostring experiments and CRISPR clone identification. E.A., K.R., Y.D., and N.P. contributed to protein extraction and WB experiments. A.P. transformed *S. aureus* strains for live-cell microscopy and contributed to bacterial counting on agar plates. J.G. performed the ELISA. ED contributed to RNA extraction in the organoid experiments.

F.V. provided ST80 WT and Δ*edinB* strains. R.C. and E.A. analyzed the results. R.C., E.A., and P.O.V. wrote the paper. J.J., H.M., F.V., and F.L. provided critical corrections to the paper. P.O.V., F.L., and J.J. obtained funding for this work and supervised the project. All authors have agreed to the final version of the paper.

Competing interests

The authors declare no competing interests.

Additional information

Supplementary information The online version contains supplementary material available at <https://doi.org/10.1038/s41467-022-34432-0>.

Correspondence and requests for materials should be addressed to Robin Caire or Paul O. Verhoeven.

Peer review information *Nature Communications* thanks Sabrina Mühlen and the other, anonymous, reviewer(s) for their contribution to the peer review of this work.

Reprints and permissions information is available at <http://www.nature.com/reprints>

Publisher's note Springer Nature remains neutral with regard to jurisdictional claims in published maps and institutional affiliations.

Open Access This article is licensed under a Creative Commons Attribution 4.0 International License, which permits use, sharing, adaptation, distribution and reproduction in any medium or format, as long as you give appropriate credit to the original author(s) and the source, provide a link to the Creative Commons license, and indicate if changes were made. The images or other third party material in this article are included in the article's Creative Commons license, unless indicated otherwise in a credit line to the material. If material is not included in the article's Creative Commons license and your intended use is not permitted by statutory regulation or exceeds the permitted use, you will need to obtain permission directly from the copyright holder. To view a copy of this license, visit <http://creativecommons.org/licenses/by/4.0/>.

© The Author(s) 2022